



1 **Late Paleocene – early Eocene Arctic Ocean Sea Surface Temperatures;**
2 **reassessing biomarker paleothermometry at Lomonosov Ridge**

3

4 Appy Sluijs¹, Joost Frieling¹, Gordon N. Inglis^{2*}, Klaas G.J. Nierop¹, Francien Peterse¹,
5 Francesca Sangiorgi¹ and Stefan Schouten^{1,3}

6

7 ¹Department of Earth Sciences, Faculty of Geosciences, Utrecht University.
8 Princetonlaan 8a, 3584 CB Utrecht, The Netherlands

9 ²Organic Geochemistry Unit, School of Chemistry, School of Earth Sciences,
10 University of Bristol, Bristol, UK

11 ³NIOZ Royal Institute for Sea Research, Department of Microbiology and
12 Biogeochemistry, and Utrecht University, PO Box 59, 1790AB Den Burg, The
13 Netherlands

14

15 * present address: School of Ocean and Earth Science, University of Southampton, UK

16

17

18



19 **Abstract**

20 The Integrated Ocean Drilling Program Arctic Coring Expedition on Lomonosov
21 Ridge, Arctic Ocean (IODP Expedition 302 in 2004) delivered the first Arctic Ocean
22 sea surface temperature (SST) and land air temperature (LAT) records spanning the
23 Paleocene-Eocene Thermal Maximum (PETM; ~56 Ma) to Eocene Thermal Maximum
24 2 (ETM2; ~54 Ma). The distribution of glycerol dialkyl glycerol tetraether (GDGT)
25 lipids indicated elevated SST (ca. 23 to 27 °C) and LATs (ca. 17 to 25 °C). However,
26 recent analytical developments have led to: i) improved temperature calibrations and
27 ii) the discovery of new temperature-sensitive glycerol monoalkyl glycerol tetraethers
28 (GMGTs). Here, we have analyzed GDGT and GMGT distributions in the same
29 sediment samples using new analytical procedures, interpret the results following the
30 currently available proxy constraints and assess the fidelity of new temperature
31 estimates in our study site.

32 The influence of several confounding factors on TEX_{86} SST estimates, such as
33 variations in export depth and input from exogenous sources, are typically negligible.
34 However, contributions of isoGDGTs from land, which we characterize in detail,
35 complicate TEX_{86} paleothermometry in the late Paleocene and part of the interval
36 between the PETM and ETM2. The isoGDGT distribution further supports temperature
37 as the likely variable controlling TEX_{86} values and we conclude that background early
38 Eocene SSTs generally exceeding 20 °C, with peak warmth during the PETM (~26 °C)
39 and ETM2 (~27 °C). We also report high abundances of branched glycerol monoalkyl
40 glycerol tetraethers throughout (branched GMGTs), most likely dominantly marine in
41 origin, and show that their distribution is sensitive to environmental parameters. Further
42 analytical, provenance and environmental work is required to test if and to what extent
43 temperature may be an important factor.



44 Published temperature constraints from branched GDGTs and terrestrial vegetation also
45 support remarkable warmth in the study section and elsewhere in the Arctic basin, with
46 vegetation proxies indicating coldest month mean temperatures of 6-13 °C. If TEX₈₆-
47 derived SSTs truly represent mean annual SSTs, the seasonal range of Arctic SST was
48 in the order of 20 °C, higher than any open marine locality in the modern ocean. If SST
49 estimates are skewed towards the summer season, seasonal ranges were comparable to
50 those simulated in future ice-free Arctic Ocean scenarios. This uncertainty remains a
51 fundamental issue, and one that limits our assessment of the performance of fully-
52 coupled climate models under greenhouse conditions.

53

54 **1. Introduction**

55 The Eocene epoch (56 to 34 million years ago; Ma) has long been characterized by
56 warm climates. The earliest signs of a balmy Eocene Arctic region – fossil leaves of
57 numerous plant species – were documented 150 years ago (Heer, 1869). Subsequent
58 findings identified palms, baobab and mangroves, indicating the growth of temperate
59 rainforests and year-round frost-free conditions in the Eocene Arctic region
60 (Schweitzer, 1980; Greenwood and Wing, 1995; Suan et al., 2017; Willard et al., 2019).
61 Fossils of animals, including varanid lizards, tortoises and alligators also indicate warm
62 Arctic climates (Dawson et al., 1976; Estes and Hutchinson, 1980). These earliest
63 findings sparked interest into the climatological mechanisms allowing for such polar
64 warmth about a century ago (Berry, 1922). Ever since, paleobotanists have focused on
65 the Arctic plant fossils and have significantly refined their paleoclimatological
66 interpretation towards estimates of precipitation as well as seasonal and mean annual
67 temperature (e.g. Uhl et al., 2007; Greenwood et al., 2010; Eberle and Greenwood,
68 2012; Suan et al., 2017; Willard et al., 2019).



69 Novel insights in Paleogene Arctic paleoclimate research were made in the years
70 following the Arctic Coring Expedition 302 (ACEX, Integrated Ocean Drilling
71 Program (IODP) 2004, Figure 1). This expedition recovered upper Paleocene and lower
72 Eocene siliciclastic sediments, deposited in a shallow marine environment, in Hole 4A
73 ($87^{\circ} 52.00$ 'N; $136^{\circ} 10.64$ 'E; 1,288 m water depth), on the Lomonosov Ridge in the
74 central Arctic Ocean (Backman et al., 2006), deposited at a paleolatitude of $\sim 78^{\circ}$ N,
75 based on a geological reconstruction (Seton et al., 2012) projected using a
76 paleomagnetic reference frame (Torsvik et al., 2012) (see paleolatitude.org, Van
77 Hinsbergen et al., 2015). The sediments are devoid of biogenic calcium carbonate, but
78 rich in immature organic matter, including terrestrial and marine microfossil
79 assemblages and molecular fossils that provided a wealth of information regarding
80 Paleocene and Eocene Arctic climates, environments, and ecosystems (Brinkhuis et al.,
81 2006; Pagani et al., 2006; Sluijs et al., 2006; Stein et al., 2006; Schouten et al., 2007b;
82 Stein, 2007; Sangiorgi et al., 2008; Sluijs et al., 2008b; Waddell and Moore, 2008;
83 Weller and Stein, 2008; Sluijs et al., 2009; Speelman et al., 2009; Speelman et al., 2010;
84 Barke et al., 2011; Barke et al., 2012; Krishnan et al., 2014; Willard et al., 2019).

85 As the upper Paleocene and lower Eocene sediments of the ACEX core lack biogenic
86 calcium carbonate and alkenones, SST reconstructions are based on the biomarker-
87 based paleothermometer TEX₈₆. This proxy is based on membrane lipids (isoprenoid
88 glycerol dibiphytanyl glycerol tetraethers; isoGDGTs) of Thaumarchaeota, which adapt
89 the fluidity of their membrane according to the surrounding temperature by increasing
90 the number of cyclisations at higher temperatures (De Rosa et al., 1980; Wuchter et al.,
91 2004; Schouten et al., 2013, and references therein). The proxy was introduced in 2002
92 by Schouten et al. (2002) and was calibrated to mean annual SST using modern marine
93 surface sediments.



94 Initial papers suggested that SST increased significantly during two episodes of
95 transient global warming. Maximum values of $\sim 23^{\circ}\text{C}$ and $\sim 27^{\circ}\text{C}$ occurred during the
96 Paleocene-Eocene Thermal Maximum (PETM-56 Ma ago, Sluijs et al., 2006) and
97 Eocene Thermal Maximum 2 (ETM2-54 Ma ago, Sluijs et al., 2009), respectively.
98 Lower SSTs, generally exceeding 20°C , characterized the remainder of the early
99 Eocene (Sluijs et al., 2008b). Such temperatures were immediately recognized to be
100 remarkably high and could not be explained using fully-coupled climate model
101 simulations (Sluijs et al., 2006). Even the current-generation of IPCC-class models are
102 unable to match early Eocene Arctic mean annual SSTs, although reconstructions of
103 tropical and mid-latitude SSTs and deep ocean temperatures are consistent with some
104 newer simulations (Frieling et al., 2017; Cramwinckel et al., 2018; Evans et al., 2018;
105 Zhu et al., 2019).

106 Since the publication of the ACEX SST records, constraints on the applicability of the
107 TEX_{86} proxy have tremendously improved (see review by Schouten et al., 2013, and
108 subsequent work by Taylor, 2013 #1645; Elling et al., 2014; Qin et al., 2014; Elling et
109 al., 2015; Kim et al., 2015; Qin et al., 2015; Hurley et al., 2016; Zhang et al., 2016).

110 This work has delivered new constraints on the ecology of Thaumarchaeota, the
111 dominant depth at which they reside in the ocean and from which depth their isoGDGTs
112 are exported towards the sea floor. Moreover, it identified potential confounding factors
113 such as variation in dominant isoGDGT export depth (e.g., Taylor et al., 2013; Kim et
114 al., 2015), the input of non-Thaumarchaeotal-derived isoGDGTs (e.g., Weijers et al.,
115 2011; Zhang et al., 2011), growth phase (Elling et al., 2014), and environmental
116 ammonium and oxygen concentrations (Qin et al., 2015; Hurley et al., 2016), and
117 several indicators to detect anomalies have been developed. In addition, improvements
118 in the chromatography method used for GDGT analysis now allow for improved



119 separation of previously co-eluting compounds leading to enhanced analytical precision
120 and sensitivity (Hopmans et al., 2016). Also, recent work has described new GDGTs
121 from oceans and sediments, notably glycerol monoalkyl glycerol tetraethers (previously
122 ‘H-shaped’ GDGTs) (e.g., Schouten et al., 2008; Liu et al., 2012), characterized by a
123 covalent carbon-carbon bond that links the two alkyl chains, that may be useful for
124 reconstructing land air temperatures (LAT) (e.g., Naafs et al., 2018a; Baxter et al.,
125 2019). However, these compounds have not yet been investigated in ancient marine
126 sediments.

127 Considering these developments and the paleoclimatological importance of the ACEX
128 dataset, we re-analyzed the original lipid extracts for the PETM, ETM2 and the interval
129 spanning these events (Sluijs et al., 2006; Sluijs et al., 2009), according to the latest
130 chromatography protocols. We also compile published and generate new GDGT data
131 from modern and Paleogene terrestrial deposits and use these to better assess the
132 potential confounding influence of isoGDGTs from terrestrial sources, which was
133 already recognized as a potential problem in the early work (Sluijs et al., 2006).

134

135 **2. GDGT-based SST indices, calibration and confounding factors**

136 *2.1 TEX₈₆ and its calibration to SST*

137 TEX₈₆ is based on the relative abundance of 4 different GDGTs (Figure 2), following
138 (Schouten et al., 2002):

$$139 \text{TEX}_{86} = \frac{([\text{GDGT-2}] + [\text{GDGT-3}] + [\text{Crenarchaeol isomer}])}{([\text{GDGT-1}] + [\text{GDGT-2}] + [\text{GDGT-3}] + [\text{Crenarchaeol isomer}])} \quad \text{Eq. (1)}$$

140 where a higher relative abundance of cyclopentane moieties implies higher SSTs.

141

142 A number of models are used to calibrate TEX₈₆ to SST (Schouten et al., 2002;
143 Schouten et al., 2003; Schouten et al., 2007a; Kim et al., 2008; Liu et al., 2009; Kim et



144 al., 2010; O'Brien et al., 2017), all based on a modern ocean surface sediment database.
145 The currently available culture and mesocosm experiments and surface sediment data
146 indeed suggest a linear relation, except for polar regions where the TEX_{86} response to
147 temperature deviates (Kim et al., 2010; Ho et al., 2014; O'Brien et al., 2017). However,
148 physiological considerations and multiple temperature-dependent GDGT indices might
149 imply a non-linear relation also at the high temperature end, as can be observed at the
150 high end of the modern ocean dataset and beyond the reach of the modern ocean
151 (Cramwinckel et al., 2018). Specifically, at higher temperatures, membrane adaptation
152 may increasingly be established using isoGDGTs not included in the TEX_{86} ratio
153 leading to a diminished TEX_{86} response at very high temperatures (Cramwinckel et al.,
154 2018). A non-linear response has thus been proposed in other calibrations (Liu et al.,
155 2009; Kim et al., 2010). The most recent non-linear calibration, TEX_{86}^H (Kim et al.,
156 2010), represents an exponential relation between SST and TEX_{86} (Hollis et al., 2019).
157 Unfortunately, TEX_{86}^H is mathematically problematic and has systematic residuals in
158 the modern ocean (Tierney and Tingley, 2014).
159 Tierney and Tingley (2014) introduced a spatially-varying Bayesian method to convert
160 TEX_{86} to SST, which assumes a linear relationship between the two (BAYSPAR). In
161 deep-time settings, BAYSPAR searches the modern core-top dataset for TEX_{86} values
162 that are similar to the measured TEX_{86} value within a user-specified tolerance and
163 draws regression parameters from these modern analogue locations. This approach
164 yields uncertainty bounds that reflect spatial differences in the slope and intercept terms
165 and the error variance of the regression model, based on the modern ocean.
166 Currently, it is generally accepted to present results both using a linear and a non-linear
167 function (Hollis et al., 2019). The assumption of a linear or non-linear relation between
168 SST and TEX_{86} leads to very different SST reconstructions for geological samples



169 yielding TEX₈₆ values beyond the modern data set (Kim et al., 2010; Tierney and
170 Tingley, 2014; Frieling et al., 2017; O'Brien et al., 2017; Cramwinckel et al., 2018).
171 However, TEX₈₆ values of the early Eocene ACEX samples (0.5 – 0.7, Sluijs et al.,
172 2006; Sluijs et al., 2008b; Sluijs et al., 2009)) are well within the modern ocean
173 calibration dataset and well above most values observed in the polar regions (Kim et
174 al., 2010; Tierney and Tingley, 2014; O'Brien et al., 2017), indicating that all
175 calibrations will yield similar absolute values.

176

177 *2.2 Caveats and confounding factors*

178 Several confounding factors and caveats have been identified that could potentially bias
179 TEX₈₆ data relative to mean annual SST. These notably relate to additions of isoGDGTs
180 that were not produced in the upper water column by Thaumarchaeota, seasonal biases,
181 and choices that are made in the calibration between SST and TEX₈₆. Below we
182 summarize methods that have been developed to assess if isoGDGT distributions might
183 have been biased by confounding factors.

184

185 *2.2.1 isoGDGTs of terrestrial origin*

186 At the time of the first ACEX papers, it was already known that high contributions of
187 terrestrially-derived isoGDGTs could compromise the TEX₈₆ signal (Weijers et al.,
188 2006). Previous work (Sluijs et al., 2006; Sluijs et al., 2008b; Sluijs et al., 2009) indeed
189 recognized that high terrestrial contributions of isoGDGTs could be problematic for
190 portions of the upper Paleocene to lower Eocene interval of the ACEX core based on
191 high BIT index values. This contribution can be tracked using the Branched and
192 Isoprenoid Tetraether (BIT) index, a ratio of mostly soil-derived branched GDGTs



193 (brGDGTs; Figure 2) and Crenarchaeol, which is dominantly marine-derived
194 (Hopmans et al., 2004; Schouten et al., 2013):

$$195 \quad BIT \text{ index} = \frac{([brGDGT-1a]+[brGDGT-11a]+[brGDGT-111a])}{([brGDGT-1a]+[brGDGT-11a]+[brGDGT-111a])+[Crenarchaeol]} \quad \text{Eq. (2)}$$

196 Most studies define a BIT value (typically 0.3 or 0.4) above which TEX₈₆-derived SST
197 are unreliable (e.g., Weijers et al., 2006). However, the threshold of 0.4 is conservative
198 in some settings and the impact of terrigenous GDGTs on reconstructed SST will
199 depend on the nature and temperature of the source catchment (Inglis et al., 2015). In
200 addition, a cut-off value based on BIT values is difficult given the relatively large
201 differences in BIT between labs, which originate from methodological differences
202 (Schouten et al., 2009). A strong linear relationship between BIT and TEX₈₆ values is
203 often taken as indication of a bias in TEX₈₆ through land-derived isoGDGTs to the
204 marine TEX₈₆ signature (e.g., Douglas et al., 2014).

205

206 *2.2.2 isoGDGTs of deep water origin*

207 Thaumarchaeota, the source of most GDGTs in marine waters (Zeng et al., 2019;
208 Besseling et al., 2020), are ammonium oxidizers (Könneke et al., 2005; Wuchter et al.,
209 2006a), making them independent of light. Although they occur throughout the water
210 column, maximum abundances are at depths <200 m, generally around NO₂ maxima
211 (e.g., Karner et al., 2001; Pitcher et al., 2011a). In most oceans, the sedimentary GDGTs
212 dominantly derive from the upper few hundred meters, based on analyses of suspended
213 particular organic matter and sediment traps (Wuchter et al., 2005; Wuchter et al.,
214 2006b; Yamamoto et al., 2012; Richey and Tierney, 2016), although some
215 contributions from deeper have sometimes been inferred based on ¹⁴C analysis (Shah
216 et al., 2008). This implies possible contributions of isoGDGTs produced in thermocline
217 waters. Moreover, contributions of isoGDGTs produced in the deep sea have regionally



218 been identified (e.g., Kim et al., 2015). Taylor et al. (2013) also found that deeper
219 dwelling archaea might contribute to the sedimentary isoGDGT assemblage. They
220 indicate that such deep contributions can be tracked using the GDGT-2/GDGT-3 ratio;
221 high values of >5 indicate contributions of archaea living deeper in the water column.
222 Given that upper Paleocene and lower Eocene ACEX sediments were deposited in a
223 shallow shelf environment (Sluijs et al., 2008b), a significant contribution of deep ocean
224 archaeal lipids is not expected.

225

226 *2.2.3 isoGDGTs of methanotrophic and methanogenic archaea*

227 Contributions of isoGDGTs to the sedimentary pool might also derive from anaerobic
228 methanotrophs and/or methanogens. Several indices have been developed to track such
229 contributions, both based on relatively high contributions of particular isoGDGTs of
230 these groups of archaea. The Methane Index (MI) was developed to detect the relative
231 contribution of anaerobic methanotrophic *Euryarchaeota* assumed to be represented by
232 GDGT-0 but also GDGT-1, 2 and 3 (Zhang et al., 2011) and is therefore defined as

$$233 \quad MI = \frac{[GDGT-1]+[GDGT-2]+[GDGT-3]}{([GDGT-1]+[GDGT-2]+[GDGT-3]+[Crenarchaeol]+[Cren.isomer])} \quad \text{Eq. (3)}$$

234 MI values greater than 0.5 indicate significant anaerobic methanotrophy. Such values
235 may yield unreliable TEX_{86} values. Another tracer for contributions of anaerobic
236 methanotrophic archaea is the analogous GDGT-2/Crenarchaeol ratio (Weijers et al.,
237 2011).

238 Methanogenic archaea can synthesize GDGT-0, as well as smaller quantities of GDGT-
239 1, GDGT-2 and GDGT-3. The ratio GDGT-0/Crenarchaeol is indicative of
240 contributions of methanogenic archaea to the isoGDGT pool (Blaga et al., 2009) where
241 values > 2 indicate substantial contribution of methanogenic archaea. Up to now, high
242 indices have often been observed near methane seeps or anoxic basins but rarely in open



243 marine waters. Given the reducing conditions in the sediment and water column at the
244 study site across the late Paleocene and early Eocene (Sluijs et al., 2006; Stein et al.,
245 2006; Sluijs et al., 2008b; März et al., 2010), an influence of methane cycling might be
246 expected.

247

248 *2.2.4 isoGDGTs of the 'Red Sea Type'*

249 Sedimentary isoGDGT distributions from the Red Sea are anomalous to that of other
250 marine settings by the low abundance of GDGT-0 and the high abundances of the
251 Crenarchaeol regio-isomer, presumably due to an endemic Thaumarchaeotal
252 assemblage, and this yields a different relationship between SST and TEX₈₆ (Trommer
253 et al., 2009; Kim et al., 2015). Inglis et al. (2015) attempted to quantify a 'Red Sea-
254 type' GDGT distribution in geological samples using the following index:

$$255 \quad \%GDGT_{rs} = \frac{[Crenarchaeol\ isomer]}{([GDGT-0] + [Crenarchaeol\ isomer])} \times 100 \quad \text{Eq. (4)}$$

256 However, as noted by Inglis et al., (2015) this ratio is also strongly SST-dependent such
257 that the Red Sea type GDGT assemblage cannot be discerned from GDGT distributions
258 that occur at high temperatures in normal open marine settings.

259

260 *2.2.5 Seasonal bias*

261 TEX₈₆ is calibrated to mean annual SST. However, particularly in mid and high latitude
262 areas where production and export production is highly seasonal, the sedimentary
263 GDGT distribution might not represent annual mean conditions (Wuchter et al., 2006b;
264 Pitcher et al., 2011b; Mollenhauer et al., 2015; Richey and Tierney, 2016; Park et al.,
265 2019). This issue should partly be reflected in the calibration uncertainty of the modern
266 ocean database (several °C, depending on the calibration and method; see section 2.7).
267 Sluijs et al. (2006; 2008b; 2009) originally argued that the TEX₈₆ results from the



268 ACEX core could be biased towards summer temperature because the export of organic
269 matter from the surface ocean towards the sediment likely peaked during the season of
270 highest production, i.e., the summer. However, we also note that the TEX_{86} -temperature
271 relationship is not improved when using seasonal mean ocean temperatures (Kim et al.,
272 2010; Tierney and Tingley, 2014) and modern observations indicate homogenization
273 of the seasonal cycle at depth (Wuchter et al., 2006b; Yamamoto et al., 2012; Richey
274 and Tierney, 2016), implying that seasonality has relatively limited effect on modern
275 sedimentary TEX_{86} values.

276

277 *2.2.6 Additional isoGDGT-based temperature indicators*

278 The underlying mechanism of TEX_{86} is that isoGDGTs produced at higher SSTs
279 contain more rings than those produced at low SSTs. Although the combination of
280 compounds included in TEX_{86} seems to yield the strongest relation with temperature in
281 the modern ocean (Kim et al., 2010), it implies that isoGDGT ratios other than TEX_{86}
282 also provide insights into SST. One alternative temperature sensitive isoGDGT index
283 is the Ring Index (RI), which represents the weighed number of cyclopentane rings of
284 isoGDGTs 0-3, Crenarchaeol and the Crenarchaeol isomer (Zhang et al., 2016), defined
285 as:

$$286 \quad RI = 0x[\%GDGT - 0] + 1x[\%GDGT - 1] + 2x[\%GDGT - 2] + 3x[\%GDGT - 3] +$$
$$287 \quad 4x[\%Crenarchaeol + \%Crenarchaeol\ isomer] \quad \text{Eq. (5)}$$

288 Note that the abundance of GDGT-0 is important for determining the percentage of the
289 other GDGTs of the total isoGDGT pool.

290 The close relation between TEX_{86} and RI can also be used to detect aberrant
291 distributions, including those produced by methanogenic, methanotrophic and
292 terrestrial sources, as these sources typically contribute disproportionate amounts of



293 specific lipids. A RI_{TEX} , calculated from TEX using the polynomial fit of Zhang et al.
294 (2016), is subtracted from the RI to arrive at the ΔRI . Cut-off values for sample
295 deviation from the modern ocean calibration dataset are defined as 95% confidence
296 limits of the RI-TEX relation, or above $|0.3| \Delta RI$ units.

297

298 *2.3 H-shaped branched GDGTs; brGMGTs*

299 H-shaped branched GDGTs (hereafter referred to as branched glycerol monoalkyl
300 glycerol tetraethers; brGMGTs; Figure 2) were first identified by Liu et al. (2012) in
301 marine sediments, who identified a single acyclic tetramethylated brGMGT (m/z 1020).
302 This compound was later detected within the marine water column and appeared to be
303 abundant within the oxygen minimum zone (Xie et al., 2014). Naafs et al. (2018a)
304 identified a larger suite of brGMGTs (including m/z 1048 and 1034), in a quasi-global
305 compilation of modern peat samples. They argued that these compounds were
306 preferentially produced at depth, within the anoxic catotelm. Analogous to the
307 continental paleothermometer based on bacterial brGDGTs produced in surface soils,
308 termed MBT'_{5me} (Weijers et al., 2011; De Jonge et al., 2014), they showed that the
309 degree of methylation of brGMGTs in peats relates to mean annual air temperature.
310 They calculated the degree of methylation of brGDGTs without cyclopentane moieties,
311 designed for comparison to the methylation of brGMGTs, defined by $H-MBT_{acyclic}$:

312

$$313 \quad MBT_{acyclic} = \frac{brGDGT-1a}{(brGDGT-1a+brGDGT-11a+GDGT-11a'+brGDGT-111a+brGDGT-111a')} \text{ Eq. (6)}$$

314

$$315 \quad H - MBT_{acyclic} = \frac{brGMGT-H1020}{(brGMGT-H1020+brGMGT-H1034+brGMGT-1048)} \text{ Eq. (7)}$$

316



317 Based on the strong relation between MBT_{cyclic} and H-MBT_{cyclic} in their peat
318 samples, Naafs et al. (2018a) suggested that the brGMGTs have the same origin as the
319 brGDGTs, presumably Acidobacteria (Sinninghe Damsté et al., 2011; Sinninghe
320 Damsté et al., 2018). In addition, they showed that the abundance of brGMGTs relative
321 to the total amount of brGMGTs and brGDGTs positively correlates with mean annual
322 air temperature, suggesting that the covalent bond in the brGMGTs is used to maintain
323 membrane stability at higher temperature (Naafs et al., 2018a).

324 Baxter et al., (2019) identified a total of seven different brGMGTs in the mass
325 chromatograms with m/z 1020, 1034 and 1048 from a suite of African lake sediments
326 (Figure 2), and found their relative distribution to correlate to mean annual air
327 temperature. Accordingly, they proposed a proxy for mean annual air temperature
328 termed brGMGT-I (see Figure 2 for the molecular structures referred to here):

$$329 \quad brGMGT - I = \frac{[H1020c]+[H1034a]+[H1034c]}{[H1020b]+[H1020c]+[H1034a]+[H1034c]+[H1048]} \quad Eq. (8)$$

330

331 **3. Material and Methods**

332 We used the polar fractions previously analyzed by Sluijs et al. (2006; 2009) from the
333 PETM through ETM2 interval at IODP Expedition 302 Hole 4A. These fractions
334 originate from a total lipid extract produced using a Dionex Accelerated Solvent
335 Extractor and fraction separations by Al₂O₃ column chromatography using
336 hexane:dichloromethane (DCM) (9:1, volume:volume) and DCM:methanol (1:1) to
337 yield the apolar and polar fractions, respectively. Polar fractions were re-dissolved in
338 hexane:isopropanol (99:1) and passed through a 0.45- μ m polytetrafluoroethylene filter.
339 This fraction was then analyzed by high-performance liquid chromatography (HPLC)
340 and atmospheric pressure chemical ionization–mass spectrometry using an Agilent
341 1260 Infinity series HPLC system coupled to an Agilent 6130 single-quadrupole mass



342 spectrometer at Utrecht University following Hopmans et al. (2016) to measure the
343 abundance of GDGTs. Based on long-term observation of the in-house standard, the
344 analytical precision for TEX_{86} is ± 0.3 °C.

345 To gain further insights into the potential impact of terrestrial isoGDGT input on TEX_{86}
346 values, we compiled isoGDGT and brGDGTs distributions from modern peats ($n = 473$,
347 Naafs et al., 2017) and early Paleogene lignites ($n = 58$, Naafs et al., 2018b). Note, the
348 fractional abundance of Crenarchaeol isomer was not reported in the early Paleogene
349 dataset of Naafs et al. (2018b). We therefore re-analyzed the polar fractions of their
350 early Paleogene lignite extracts via HPLC-MS using a ThermoFisher Scientific Accela
351 Quantum Access at the University of Bristol following Hopmans et al. (2016). Based
352 on long-term observation of the in-house standard, the analytical precision for TEX_{86}
353 is ± 0.3 °C for both labs.

354

355 **4. Results**

356 The new GDGT distributions (Supplementary Table) are consistent with the TEX_{86} and
357 BIT index data generated over a decade ago using the old analytical HPLC setup
358 (Hopmans et al., 2000; Hopmans et al., 2016) (Figure 3). TEX_{86} exhibits some scatter
359 but the slope of the regression is 0.98 for the entire dataset, which is indistinguishable
360 from the 1:1 line. The scatter is minor compared to the uncertainties inherent to
361 calibrations that transfer these values to SST. Less scatter is apparent in the BIT record
362 but the original BIT index values were slightly higher at the higher end recorded here
363 (~ 0.5), indicated by a shallower slope of the regression (0.92), consistent with previous
364 analyses with the new analytical setup (Hopmans et al., 2016). This does not impact
365 previous qualitative interpretations of this record (Sluijs et al., 2006; Sluijs et al., 2008b;
366 Sluijs et al., 2009). In the discussion section, we assess indicators of potential



367 confounding factors (section 2.2), including the influx of terrestrially-derived
368 isoGDGTs to the sediments (Figures 4, 5 and S1) and several indices related to methane
369 and depth of production (Figures 6).

370 Although we did not detect significant amounts of isoprenoid GMGTs, high
371 abundances of various brGMGTs, in total between 10 and 45% of the total brGDGT
372 assemblage (Figure 7), are present in the ACEX samples. Specifically, we can
373 consistently identify at least 5 peaks across the mass chromatograms of m/z 1020, 1034
374 and 1048. Based on their (relative) retention times and overall distribution we were able
375 to apply the nomenclature of Baxter et al. (2019) to 5 of these and assign individual
376 peaks to previously identified compounds (Figure S2). Abundances of brGMGTs
377 relative to brGDGTs increase during the PETM. Furthermore, the proposed temperature
378 indicators based on brGMGTs show mixed results, with some showing a clear response
379 to the PETM (Figure 7d) while others do not (Figure 7e).

380

381 **5. Discussion**

382 *5.1 IsoGDGT provenance*

383 *5.1.1 Contributions of soil-derived isoGDGTs*

384 As noted by Sluijs et al. (2006), Paleocene samples yield anomalously high abundances
385 of GDGT-3, likely derived from a terrestrial source. To assess the temperature change
386 during the PETM, they therefore explored a TEX_{86} calibration without this moiety,
387 termed TEX'_{86} . However, TEX'_{86} has not been widely used outside the Paleogene Arctic
388 because the anomalous abundances of GDGT-3 have not been recorded elsewhere. In
389 addition, high contributions of GDGT-3 from terrestrial input would also be associated
390 with an increase in the abundance of other isoGDGTs. We therefore consider the late
391 Paleocene temperature estimates unreliable. Indeed, recent TEX_{86} -based global SST



392 compilations and comparison to climate simulations for the PETM excluded the ACEX
393 record because the TEX_{86} ' calibration complicates the comparison to other regions
394 (Frieling et al., 2017; Hollis et al., 2019) and has not been applied elsewhere.
395 Input of soil organic matter is consistent with Willard et al. (2019) who established that
396 the brGDGT assemblage is dominantly soil derived as opposed to being produced in
397 the coastal marine environment (Sinninghe Damsté, 2016). This observation is based
398 upon the weighted average number of rings in the tetramethylated brGDGTs ($\#rings_{\text{tetra}}$)
399 which generally does not exceed 0.4 to 0.7 in the global soil calibration dataset
400 (Sinninghe Damsté, 2016). In the ACEX record, $\#rings_{\text{tetra}}$ is always below 0.21
401 (Willard et al., 2019), consistent with a dominant soil source. This indicates that
402 brGDGT abundances, brGDGT distributions and the BIT index are reliable indicators
403 of the relative supply of terrestrially-derived isoGDGTs into the marine basin.
404 The Paleocene section of the dataset also stands out regarding its relation between BIT
405 index and TEX_{86} (Figure 4), which confirms its anomalous nature. During the PETM,
406 TEX_{86} values are higher due to warming and BIT values lower, which was attributed to
407 sea level rise during the hyperthermals resulting in a more distal position relative to the
408 terrestrial GDGT source (Sluijs et al., 2006; Sluijs et al., 2008a). From the remainder
409 of the dataset, the interval between 371.0 and 368.0 mcd, just below ETM2, stands out.
410 This interval was previously recognized by Sluijs et al. (2009) to reflect the most open
411 marine environment in the studied section, with dominant marine palynomorphs and
412 biomarkers. They also found that high BIT values correspond to low TEX_{86} values
413 within that interval and therefore they implemented a subjective cut-off BIT value of
414 0.3, above which TEX_{86} -derived SSTs were considered unreliable. Although the
415 relation between BIT and TEX_{86} exhibits much scatter, the new analyses supports the
416 notion that higher influx of terrestrial isoGDGTs lowers TEX_{86} values, explaining 26%



417 of the variation in a linear regression (Figure 4). The nature of this influence is
418 determined by the relative abundance of terrestrial isoGDGTs and their TEX_{86} value.
419 The TEX_{86} value at the terrestrial endmember of $BIT = 1$, assuming various types of
420 relations, centers around 0.5. The remainder of the data does not show a clear relation
421 between BIT and TEX_{86} although some of the lowest TEX_{86} values correspond to high
422 BIT values, suggesting that the terrestrial endmember contributed isoGDGT
423 assemblages with relatively low TEX_{86} values in other intervals as well.
424 Interestingly, the relatively low degree of cyclization of soil-derived isoGDGTs in the
425 early Eocene contrasts starkly with the anomalous contributions of GDGT-3 in the
426 Paleocene. This implies that the distribution of supplied terrestrial isoGDGTs differed
427 strongly between the Paleocene and Eocene part of the studied section.
428 The impact of soil-derived isoGDGTs also emerges from the Ring Index approach of
429 Zhang et al. (2016, see section 2.6). The difference between the Ring Index and TEX_{86}
430 at the onset of the PETM is mainly controlled by Crenarchaeol, which is comparatively
431 low in abundance in the Paleocene but highly abundant in the PETM. This increase is
432 likely associated with sea level rise during the PETM because Crenarchaeol is
433 predominantly produced in the marine realm. It is also consistent with a drop in BIT
434 index values and the relative abundance of terrestrial palynomorphs (Sluijs et al.,
435 2008a). The approach of Zhang et al. (2016) also confirms that many isoGDGT
436 distributions exhibit an anomalous relation between TEX_{86} and the Ring Index relative
437 to the modern core top dataset, with ΔRI values >0.3 (Figure 6). Importantly, all
438 samples with ΔRI values >0.3 have BIT values above 0.35, indicating that contributions
439 of soil-derived iso-GDGTs dominate non-temperature effects in the distributions. We
440 therefore discard TEX_{86} -derived SSTs for samples with BIT values >0.35 .
441



442 We attempt to further constrain the potential contribution of terrestrially-derived
443 isoGDGTs by determining the abundance of isoGDGTs relative to brGDGTs in modern
444 peat samples (Naafs et al., 2017) and early Paleogene lignites (Naafs et al., 2018b, the
445 isoGDGT data are published here). The absolute concentrations of brGDGTs in the
446 ACEX samples are then used to estimate the potential contribution of terrestrially-
447 derived isoGDGTs to the samples. To this end, we use the fractional abundance of the
448 various isoGDGTs in available global terrestrial sediment calibration datasets,
449 specifically modern peats and Paleogene lignites (Figure 5). Then, we estimate the
450 abundance of these terrestrially-derived isoGDGTs in our ACEX samples by scaling
451 this fraction to the measured abundances of brGDGTs and isoGDGTs in our ACEX
452 samples, following

453 *Terrestrial fraction of isoGDGT n =*

454 $(\text{Fraction of isoGDGT } n \text{ in terrestrial test dataset} * \frac{\text{sum(brGDGTs)}}{\text{abundance of isoGDGT } n})$ Eq. (9)

455 where n represents the specific analyzed GDGT.

456 This leads to estimates of the potential relative contributions of the individual
457 isoGDGTs derived from land in the ACEX samples based on the entire modern peat
458 dataset (Naafs et al., 2017), modern peats from regions with MAT exceeding 15°C
459 (Naafs et al., 2017) and Paleogene lignites (Naafs et al., 2018b, this paper, Figures 5
460 and S1). This shows that Crenarchaeol and Crenarchaeol-isomer remain almost
461 exclusively marine even with high brGDGT concentrations. However, we show that
462 GDGT-1, GDGT-2 and GDGT-3 all have potentially large terrestrial contributions in
463 the ACEX samples (Figure 5), more concentrated in specific stratigraphic intervals
464 (Figure S1). In the most extreme cases, the modeled contributions of terrestrial
465 isoGDGTs, based on the measured brGDGTs and modern peat dataset is higher than
466 the actually measured isoGDGT abundances (terrestrial fraction higher than 1). This is



467 principally seen in iGDGT-2 and 3, and predominantly when we calculate the isoGDGT
468 contribution using the Paleogene lignite database. This particular assumption thus
469 clearly leads to overestimates of the amount of terrestrially sourced isoGDGTs in our
470 setting. However, the trends between the modern peats, warm modern peats and
471 Paleogene lignites are essentially identical and give some indication which isoGDGTs
472 are most likely to be affected and across which intervals.

473 Interestingly, particularly GDGT-3 is shown to be affected in ACEX samples if the
474 terrestrial contribution of isoGDGTs is analogous in distribution to that of warm
475 modern peats and/or Paleogene lignites (Figure 5), which qualitatively matches the
476 distributions in the ACEX samples. This is principally because GDGT-3 is the least
477 abundant marine isoGDGT included in our analyses, whereas it is often as abundant as
478 GDGT-1 and 2 in terrestrial settings (Fig. 5).

479

480 *5.1.2 Contributions of methanotrophic or methanogenic archaea?*

481 The depositional environment at the study site, with ample (export) production,
482 sediment organic matter content, and low oxygen conditions at the sediment-water
483 interface (Sluijs et al., 2006; Stein et al., 2006; Stein, 2007; Sluijs et al., 2008b; Sluijs
484 et al., 2009; März et al., 2010), may have been suitable for abundant methanogenic and
485 methanotrophic archaea, potentially contributing to the sedimentary isoGDGT
486 assemblage. However, our GDGT-2/Crenarchaeol values (<0.23; Figure 6) are far
487 below values that suggest significant isoGDGT contributions of methanotrophic
488 *Euryarchaeota* as described by Weijers et al. (2011). Also MI values (maximum
489 observed 0.31) are generally below proposed cut off values (0.3-0.5, Zhang et al., 2011)
490 that suggest such contributions. Finally, GDGT-0/Crenarchaeol ratios (<1.4) remain



491 below the cut-off value of 2 throughout the section (Figure 6), also making a significant
492 isoGDGT contribution from methanogens highly unlikely (Blaga et al., 2009).

493

494 *5.1.3 Contributions of deep-dwelling archaea?*

495 Taylor et al. (2013) showed that GDGT-2/GDGT-3 ratios correspond to depth of
496 production, with high values (>5) where water depth is >1000 m. We record values
497 between 1 and 4 from the bottom of the study section up to ~371.2 mcd (Figure 6),
498 which supports a dominant production in the surface ocean based on the modern
499 calibration data set (Taylor et al., 2013). However, the overlying interval up to ~368.3
500 mcd has much higher values and also highly variable values averaging 7.4 and with
501 peak values of 10-14. Such values suggest significant contributions of isoGDGTs
502 produced at water depths of several kilometers according to the analyses by Taylor et
503 al. (2013).

504 However, all paleoenvironmental information generated based on the sediments as well
505 as tectonic reconstructions of Lomonosov Ridge – a strip of continental crust that
506 disconnected from the Siberian margin in the Paleocene - has indicated a neritic setting
507 of the drill site at least up to the middle Eocene (e.g., O'Regan et al., 2008; Sangiorgi
508 et al., 2008; Sluijs et al., 2008a; Sluijs et al., 2009). Although a drop in BIT index and
509 a change in the palynological assemblages support a change towards a somewhat more
510 distal position relative to the shoreline at ~371.2 mcd, the sediment remains dominantly
511 siliciclastic and organic terrestrial components, particularly pollen and spores, remain
512 abundant (Sluijs et al., 2008a; Sluijs et al., 2008b). The high GDGT-2/GDGT-3 ratio
513 values can therefore not be explained by contributions of deep dwelling archaea.
514 Indeed, increased contributions of isoGDGTs produced at depth would be expected to
515 have caused a systematic cold bias. However, based on linear regression analysis the



516 large variability in GDGT-2/GDGT-3 ratios is unrelated to the recorded variability in
517 TEX₈₆ values.

518 Intriguingly, in a study of the last 160 kyr in the South China Sea, Dong et al. (2019)
519 found that very high GDGT-2/GDGT-3 ratios (~9 but up to 13) correspond with high
520 values in nitrogen isotope ratios, interpreted to reflect low contributions in diazotroph
521 N₂ fixation and enhanced upwelling. In our records, the high GDGT-2/GDGT-3 ratios
522 are associated with normal marine conditions and the dinocyst assemblages are not
523 indicative of upwelling conditions (Sluijs et al., 2009). Unfortunately, the available
524 nitrogen isotope record (Knies et al., 2008) does not cover our study interval in
525 sufficient resolution to assess a relation with diazotroph activity. As such, the cause of
526 the high GDGT-2/GDGT-3 ratios in this interval remains unclear but we consider it
527 highly unlikely to relate to contributions of very deep dwelling Thaumarchaeota.

528

529 *5.1.4 Oxygen concentrations and ammonium oxidation rates*

530 A variety of non-thermal factors can impact TEX₈₆ values, including ammonium and
531 oxygen concentrations and growth phase (Elling et al., 2014; Qin et al., 2014; Hurley
532 et al., 2016). Across the studied interval of the ACEX core, several intervals of seafloor
533 and water column anoxia have been identified based on organic and inorganic proxies,
534 notably during the PETM and ETM2 (Sluijs et al., 2006; Stein et al., 2006; Sluijs et al.,
535 2008b; Sluijs et al., 2009; März et al., 2010).

536 Particularly suspect is an interval of low TEX₈₆ values that marks the middle of the
537 ETM2 interval, directly following a ~4 °C warming at its onset (Sluijs et al., 2009).
538 This interval is also marked by the presence of sulfur-bound isorenieratane (Sluijs et
539 al., 2009), a derivative of isorenieratene, a biomarker produced by the brown strain of
540 green sulfur bacteria that require light for photosynthesis and free sulfide, indicating



541 euxinic conditions in the (lower) photic zone (Sinninghe Damsté et al., 1993). We also
542 record a concomitant shift in several methane-related indicators, GDGT-2/GDGT-3
543 ratio values and the Δ RI. A mid-ETM2 cooling signal has not been recorded at other
544 study sites and this interval marks the occurrence of pollen of thermophilic plants such
545 as palms and baobab (Sluijs et al., 2009; Willard et al., 2019). Therefore, the low TEX_{86}
546 values were suggested to reflect thaumarcheotal depth migration to the deeper
547 chemocline due to euxinic conditions (Sluijs et al., 2009), similar to the modern Black
548 Sea (Coolen et al., 2007; Wakeham et al., 2007) and the Mediterranean Sea during
549 sapropel formation (Menzel et al., 2006).

550 More recent work has indicated that the isolated marine Thaumarchaeotal species
551 *Nitrosopumilus maritimus* produces lower TEX_{86} values with higher ammonia
552 oxidation rates (Hurley et al., 2016) and O_2 concentrations (Qin et al., 2015). Although
553 this observation is difficult to extrapolate to the total response of the Thaumarcheotal
554 community in the marine environment on geological time scales, lower O_2 availability
555 should lower oxidation rates leading to higher TEX_{86} values (Qin et al., 2015; Hurley
556 et al., 2016). However, we record a drop in TEX_{86} values with the development of
557 anoxia during ETM2. The nature of the anomalously low cyclization in the ETM2
558 isoGDGT assemblage, which pass all quality tests regarding GDGT distribution (Figure
559 6), remains therefore elusive. In general, however, if the relatively restricted and low-
560 O_2 setting had any impact on TEX_{86} values, these culture studies (Qin et al., 2015;
561 Hurley et al., 2016) suggest it would have led to an underestimate of the SST.

562

563 *5.2 Origin and environmental forcing of brGMGTs*

564 The relative abundances of brGMGTs in our samples are surprisingly high. On average,
565 they comprise 25% of the total branched GDGT and GMGT assemblage. The limited



566 literature on modern occurrences implies that both terrestrial and marine sources may
567 have contributed to the brGMGT assemblage. Data from the marine sediments (Liu et
568 al., 2012) and the water column (Xie et al., 2014), clearly shows production within the
569 marine realm. Their occurrence in modern peats (Naafs et al., 2018a), lake sediments
570 (Baxter et al., 2019) and Paleogene lignites (Inglis et al., 2019) might also imply
571 transport from land to marine sediments. A soil-derived source is currently
572 unsupported, as they were most often below detection limit in recent studies of
573 geothermally heated soils (De Jonge et al., 2019) and a soil transect from the Peruvian
574 Andes (Kirkels et al., 2020). The brGMGT abundances we record are close to the
575 maximum abundance found in modern peats (Naafs et al., 2018a). However, significant
576 input of peat-derived organic matter into our study site is inconsistent with the low input
577 of peat-derived *Sphagnum* spores (Willard et al., 2019). Alternatively, the high
578 abundance of brGMGTs could also be related to subsurface production, which was
579 invoked by Naafs et al. (2018a) to explain very high abundance of brGMGTs in an early
580 Paleogene lignite. Collectively, however, we argue that production in the marine realm
581 may be an important contributor to the brGMGT pool in our setting.

582 Several factors may contribute to the rise in the abundance of brGMGTs relative to
583 brGDGTs across the PETM. Higher relative abundances of brGMGTs in modern peats
584 generally occur at higher mean annual air temperatures (Naafs et al., 2018a) and so this
585 signal could relate to warming during the PETM if their origin at the study site is
586 terrestrial. However, we consider it likely that a large part of the brGMGTs assemblage
587 is of marine origin. If so, the rise in brGMGT abundance likely relates to the previously
588 recorded (Sluijs et al., 2006; Sluijs et al., 2008b) sea level rise during the PETM at the
589 study site, causing an increase in marine brGMGT production relative to terrestrial
590 brGDGT supply to the study site. This is consistent with the inverse correlation between



591 brGMGT abundance and the BIT index (Figure 7). Lastly, if the production of marine
592 brGMGTs was focused in oxygen minimum zones (Xie et al., 2014), the development
593 of low oxygen conditions in the water column based on several indicators, such as the
594 presence of isorenieratane (Sluijs et al., 2006), might have increased the production of
595 brGMGTs in the water column. It is also possible that all of these factors contributed
596 to the changes in abundance of brGMGTs relative to brGDGTs across the PETM.
597 The brGMGT-I proxy does not produce temperature trends similar to those seen in
598 TEX₈₆ or MBT'_{5me} (Figure 7e). If the majority of the brGMGTs is of marine origin, this
599 indicates that brGMGTs produced in the marine realm do not respond to temperature
600 as was hypothesized based on the African Lake dataset by Baxter et al. (2019).
601 Also the application of the H-MBT_{cyclic} index (equation 7) appeared problematic
602 because, similar to Baxter et al. (2019), we identified several more different isomers
603 than Naafs et al. (2018a, who developed this index) detected in their peat samples. It
604 therefore remains unclear which of our peaks should be used to calculate the H-
605 MBT_{cyclic} index values. We therefore show the two plausible options. For the first,
606 we use all peaks with m/z 1020, 1034 and 1048 (HMBT all in Figure 7) within the
607 expected retention time window. However, based on our chromatography, we consider
608 it more likely that the dominant peaks identified by Naafs et al. (2018a) at m/z 1020 and
609 1034 represent H1020c and H1034b, respectively, and therefore use only those in
610 addition to the single identifiable peak at m/z 1048 as a second option. Both options
611 show a clear rise across the PETM, although the HMBT (H1020c, H1034a) shows a
612 larger signal and somewhat better correspondence in absolute values to MBT_{cyclic},
613 though with more scatter. A close correspondence between MBT_{cyclic} and HMBT
614 was also found in a recent analysis of a lignite that seems to correspond to the PETM,



615 although interestingly, no apparent relation with temperature was found (Inglis et al.,
616 2019).

617 If a pronounced part of brGMGTs within the terrestrially-dominated Paleocene part of
618 the section is of terrestrial origin, it is possible that the drop in the relative contribution
619 of terrestrially-derived versus marine brGMGTs influenced these records. However, if
620 the dominant source of the brGMGTs was marine throughout the record, the increase
621 in methylation possibly relates to warming. This would not be unprecedented as marine-
622 produced brGDGTs show an increase in methylation as a function of temperature
623 (Dearing Crampton-Flood et al., 2018), and also isoprenoid GMGTs produced in
624 marine sediments by archaea (below detection in our samples) incorporate additional
625 methyl groups at higher sediment temperatures (Sollich et al., 2017). However, along
626 with the unresolved brGMGT sourcing, during the PETM at the study site also water
627 column oxygen concentrations and pH changed, which potentially affected
628 distributions. Extensive evaluation of brGMGT distributions in modern samples is
629 therefore required to assess the proxy potential.

630

631 *5.3 Uncertainty on TEX_{86} -based SST estimates.*

632 *5.3.1 Uncertainty based on calibration dataset*

633 To calculate SSTs, we use the BAYSPAR method (Tierney and Tingley, 2014) – which
634 assumes a linear relationship between TEX_{86} and SST - and TEX_{86}^H (Kim et al., 2010)
635 – which assumes a non-linear relationship between TEX_{86} and SST. Differences
636 between these calibrations are smaller than the calibration errors (Figure 6) because the
637 TEX_{86} values in the ACEX dataset all fall well within the range of the modern core top
638 calibration. Collectively, taken at face value, the data imply that mean annual SSTs



639 varied between 18 °C and 28 °C in the early Eocene, providing strong evidence for
640 remarkable early Eocene warmth in the Arctic region.

641 The TEX_{86}^H calibration implies a calibration error of 2.5 °C (residual mean standard
642 error; RSME) (Kim et al., 2010). The BAYSPAR method yields possible values that
643 range ~6 °C from the most probable value (Figure 6), but these uncertainty estimates
644 are more comparable than is immediately apparent as this analysis takes a 90%
645 confidence interval compared to the 68% probability of RSME. However, all of the
646 calibrations and methods to obtain values and uncertainties are based on a modern core-
647 top dataset and thus implicitly include potential confounding factors such as seasonality
648 and depth of production and export. However, there is no (quantitative) constraint on
649 any of these parameters in the calibration data set. This is particularly important for the
650 studied region because it represents a polar endmember of the marine environment with
651 highly seasonal production and export and potentially high seasonality in temperature.

652 In the modern ocean, relations between SST and TEX_{86} in the Arctic and ice-proximal
653 Southern Ocean settings differ from the global ocean, attributed to a change in
654 viscoelastic adaptation to temperature at the low end and/or a change in the
655 Thaumarchaeotal community (Kim et al., 2010; Ho et al., 2014; Tierney and Tingley,
656 2014). This may mask potential confounding factors that may be relevant specifically
657 to polar environments. This is important for our case, a situation in which the polar
658 regions were ice free and the functioning of physical, chemical and biological ocean
659 systems were fundamentally different from present day. This implies that any
660 uncertainty calculated based on the modern database, regardless whether it is done
661 based on traditional regression analyses or BAYSPAR, has no direct value for
662 determination of uncertainty in our case because the caveats and confounding factors



663 do not influence uncertainty in the same way in the Eocene as in the modern.

664 Quantification of uncertainty is at this point, therefore, extremely difficult.

665

666 *5.3.2 Constraints from independent proxy data*

667 Independent proxy data may provide additional constraints. The appearance of the

668 dinoflagellate cyst genus *Apectodinium* during the PETM and ETM2 in the Arctic basin

669 (Sluijs et al., 2006; Sluijs et al., 2009; Harding et al., 2011) provide qualitative support

670 for pronounced warming and apparent subtropical conditions. Recent efforts to quantify

671 the paleoecological affinities of this now extinct genus have suggested a required

672 minimum temperature of $\sim 20^{\circ}\text{C}$ (Frieling et al., 2014; Frieling and Sluijs, 2018).

673 Although this value is partly based on TEX_{86} data from the ACEX cores, it is supported

674 by data from an epicontinental site in Siberia (Frieling et al., 2014).

675 A second line of independent proxy evidence includes vegetation reconstructions. As

676 indicated above, the TEX_{86} results are qualitatively consistent with the ample evidence

677 for thermophilic plants and animals in the Arctic (e.g., Heer, 1869; Schweitzer, 1980;

678 Greenwood and Wing, 1995; Uhl et al., 2007; Suan et al., 2017). Particularly valuable

679 are minimum winter temperature tolerances for specific plant species. Palynological

680 analyses have indicated the presence of palm and baobab pollen within the PETM and

681 ETM2 intervals in the ACEX cores (Sluijs et al., 2009; Willard et al., 2019). Modern

682 palms are unable to tolerate sustained intervals of frost whilst sexual reproduction is

683 limited to regions where the coldest month mean temperature is significantly above

684 freezing (Van der Burgh, 1984; Greenwood and Wing, 1995). The latter was recently

685 quantified to be $\geq 5.2^{\circ}\text{C}$ (Reichgelt et al., 2018). The presence of baobab within the

686 PETM interval and ETM2 support mean winter air temperatures of at least 6°C

687 (Willard et al., 2019). Importantly, these plants were not encountered in the intervals



688 outside the PETM and ETM2, suggesting background coldest month mean air
689 temperatures were potentially too low ($<6^{\circ}\text{C}$) to support these megathermal vegetation
690 elements.

691 Pollen of palms and *Avicennia* mangroves were recently identified in time-equivalent
692 sections in Arctic Siberia (Suan et al., 2017). Although the details of stratigraphic
693 context of these records may be somewhat problematic, these findings provide good
694 evidence for very high coldest month mean temperatures, both air ($>5.5^{\circ}\text{C}$) and SST
695 ($>13^{\circ}\text{C}$) during the late Paleocene and early Eocene (Suan et al., 2017).

696 Apparently conflicting evidence comes from the occurrence of glendonites and erratics
697 in specific stratigraphic levels in Paleocene and Eocene strata in Spitsbergen,
698 interpreted to reflect cold snaps in climate (Spielhagen and Tripathi, 2009). Some of
699 these stratigraphic levels are very close to (or even potentially within) the PETM,
700 considering the local stratigraphic level of the PETM (Cui et al., 2011; Harding et al.,
701 2011), although glendonites and erratics have not been found at the exact same
702 stratigraphic levels as thermophilic biota (Spielhagen and Tripathi, 2009). The formation
703 and stability of ikaite (the precursor mineral of the diagenetic glendonites) in
704 Spitsbergen was dependent on relatively low temperature, arguably persistent near-
705 freezing sea water temperatures in the sediment (Spielhagen and Tripathi, 2009).
706 However, glendonite occurrences, some also in Mesozoic sediments in mid-latitude
707 regions, have recently also been linked to methane seeps and so the specific temperature
708 constraints implied by glendonites under such conditions are subject of debate (e.g.,
709 Teichert and Luppold, 2013; Morales et al., 2017). Clearly, however, the glendonite
710 occurrences may imply episodes of colder climates and follow up work should apply
711 temperature reconstructions based on biomarkers or biota on corresponding strata to
712 assess proxy consistency.



713 This estimate on seasonal minima provides an important constraint on Arctic
714 climatology during the PETM and ETM2. Most likely, the palms and baobabs grew
715 close to the shore, where the relative heat of the ocean kept atmospheric temperatures
716 relatively high during the winter. If minimum winter SSTs were in the range of the SST
717 reconstructions based on the nearby *Avicennia* mangrove pollen (Suan et al., 2017),
718 which for open ocean settings would perhaps amount to ~ 10 °C, then summer SST must
719 have soared to at least 30 °C in summer if TEX₈₆-based SST reconstructions of ~ 20 °C
720 truly reflects the annual mean. It would imply an SST seasonality of ~ 20 °C, much
721 higher than any modern open marine setting, let alone the Arctic Ocean. In the present
722 day Arctic Ocean, heat is seasonally stored and released in sea ice melting and freezing,
723 and sea ice cover insulates the ocean and reflects much sunlight, resulting in a seasonal
724 cycle of not more than 1.5 °C, even in ice-free regions (Chepurin and Carton, 2012).
725 However, coupled model simulations have indicated that the future loss of sea ice will
726 greatly enhance the seasonal SST range to up to 10 °C in 2300 given unabated CO₂
727 emissions (Carton et al., 2015). With year-round snow and ice-free conditions, even
728 stronger summer stratification during the Eocene due to higher greenhouse gas
729 concentrations and fresh-water supply through an enhanced hydrological cycle
730 (Pierrehumbert, 2002), a near-shore 20 °C seasonal cycle in Arctic Ocean SST may not
731 be unrealistic, although it remains inconsistent with current-generation fully coupled,
732 relatively low resolution, model simulations (e.g., Frieling et al., 2017).
733 Constraints from the total pollen assemblages in the ACEX cores based on a nearest
734 living relative approach suggest Arctic mean annual temperatures on land of 13-18 °C,
735 and summer temperatures significantly exceeding 20 °C during the PETM and ETM2
736 (Willard et al., 2019). Although these estimates come with much larger uncertainty than
737 winter temperatures and may suffer from the non-analogous setting, they are generally



738 lower than our TEX_{86} values. Also the brGDGT-based paleothermometer $\text{MBT}'_{5\text{me}}$ (De
739 Jonge et al., 2014) indicates lower temperatures mean annual air temperatures than
740 reported from TEX_{86} (Willard et al., 2019, Figure 7). These data, derived from the same
741 UHPLC/MS analyses as the isoGDGT data presented here, indicate mean annual air
742 temperatures averaging $\sim 18^\circ\text{C}$ during the PETM, with a residual mean calibration error
743 of 4.8°C . This value is $\sim 7^\circ\text{C}$ lower than earlier estimates based on a slightly different
744 method, analytical procedure and a smaller modern calibration dataset (Weijers et al.,
745 2007).

746

747 *5.4 State of constraints on Paleocene-Eocene Arctic temperatures*

748 To unlock the unique premise of Eocene climates for testing the skill of current-
749 generation fully coupled climate models under high greenhouse gas forcing, proxy data
750 and models are ideally approached separately. Among the most important implications
751 of the Arctic temperature estimates are reconstructions of the meridional temperature
752 gradients. Importantly, not a single simulation using an IPCC-class model of early
753 Paleogene climate has produced Arctic annual mean sea surface temperatures close to
754 the ACEX TEX_{86} -based reconstructions without unrealistically high tropical SSTs
755 (Lunt et al., 2012). Recent simulations using the Community Earth System Model 1
756 (CESM-1) using Eocene boundary conditions produced climates that correspond to
757 SST reconstructions in many ocean regions based on several proxies, but still produced
758 cooler mean annual SSTs for the Arctic Ocean than suggested by TEX_{86} (Frieling et al.,
759 2017; Cramwinckel et al., 2018; Zhu et al., 2019). TEX_{86} also indicates SSTs higher
760 than in these model simulations at several sites along the Antarctic margin (Bijl et al.,
761 2009; Bijl et al., 2013). The question thus remains if the conversion of TEX_{86} values
762 towards mean annual SST using any modern core-top calibration for high latitude



763 Paleogene locations is valid, or if the climate models still significantly underestimate
764 polar temperatures. Certainly, if interpreted as mean annual SST, TEX₈₆-based
765 estimates are high compared to the few available additional estimates, notably based on
766 vegetation, but the latter also suffer from similar uncertainties.

767 A few biases might exaggerate meridional temperature gradients as indicated from
768 TEX₈₆. First, the flat Eocene temperature gradient implied by TEX₈₆ was suggested to
769 result from erroneously calibrating the proxy to SST rather than to the temperature of
770 the subsurface (Ho and Laepple, 2016). The rationale is that the meridional temperature
771 gradient is smaller in deeper waters than it is in the surface. However, the idea was
772 contested for multiple reasons, including the fact that sediments at most Eocene study
773 sites, such as the ACEX site, were deposited at a depth of less than 200 m, making the
774 application of a deep subsurface (>1000m) calibration inappropriate (Tierney et al.,
775 2017). Moreover, recent analyses have indicated that the TEX₈₆ signal dominantly
776 reflects temperature of top 200 m of the water column (Zhang and Liu, 2018).

777 Secondly, as suggested previously (Sluijs et al., 2006), if TEX₈₆ were biased towards
778 any season in the non-analogue Arctic Ocean, it would be the summer, the dominant
779 season of organic matter export towards the seafloor through fecal pelleting or marine
780 snow aggregates. Vegetation suggests very high winter continental coldest month mean
781 air temperatures of at least 6-8 °C (Sluijs et al., 2009; Suan et al., 2017; Willard et al.,
782 2019), coastal coldest month mean SSTs of >13 °C (Suan et al., 2017), and terrestrial
783 mean annual and warmest month mean temperature on land of 13-21 °C and >20°C,
784 respectively (Suan et al., 2017; Willard et al., 2019) (see section 5.3.2). These estimates
785 are closer to the most recent model simulations and lower than the existing TEX₈₆ (e.g.,
786 Zhu et al., 2007; Frieling et al., 2017). If TEX₈₆-implied SST of ~25 °C is skewed
787 towards a summer estimate, this would decrease the model-data bias regarding the



788 meridional temperature gradient estimates. Given the current uncertainties in the use of
789 TEX_{86} for the non-analogue Arctic Ocean, we however cannot independently constrain
790 this.

791

792 **6. Conclusions**

793 We analyzed isoGDGT and brGMGT (H-shaped branched GDGT) distributions in
794 sediments recovered from the Paleocene-Eocene Thermal Maximum (PETM; ~56 Ma)
795 to Eocene Thermal Maximum 2 (ETM2; ~54 Ma) interval on Lomonosov Ridge, Arctic
796 Ocean using state-of-the-art analytical procedures, compare them to the original dataset
797 (Sluijs et al., 2006; Sluijs et al., 2009) and interpret the results following the currently
798 available TEX_{86} proxy constraints.

799 Although contributions of isoGDGTs from land complicate TEX_{86} paleothermometry
800 in some stratigraphic intervals, temperature was the dominant variable controlling
801 TEX_{86} values. Background early Eocene SSTs exceed ~20 °C and peak warmth
802 occurred during the PETM and ETM2. However, uncertainty estimates of these SSTs
803 based on the non-analogue modern ocean, remains complex. Temperature constraints
804 from terrestrial vegetation support remarkable warmth in the study section and
805 elsewhere in the Arctic basin, notably coldest month mean temperatures around 10 °C
806 at least within the PETM and ETM2. If TEX_{86} -derived SSTs of ~20 °C truly represent
807 mean annual SSTs, the seasonal range of Arctic SST might have been in the order of
808 20 °C. If SST estimates are entirely skewed towards the summer season, seasonal
809 ranges in the order of 10 °C may be considered comparable to those simulated in future
810 ice-free Arctic Ocean scenarios.

811 We find abundant brGMGTs, which appear predominantly produced in the marine
812 realm at the study site. Their abundance increases during the PETM, likely due to sea



813 level rise and perhaps due to warming and a drop in seawater oxygen concentrations.
814 Although speculative, an increase in brGMGT methylation during the PETM may be a
815 function of temperature, but a relation between brGMGT distribution and
816 environmental parameters including temperature is yet to be confirmed.

817

818 **6. Data Availability**

819 All data is provided in the Supplement Table and will be included in the PANGAEA
820 database upon publication of this paper.

821

822 **7. Sample Availability**

823 Requests for materials can be addressed to A.Sluijs@uu.nl

824

825 **8. Author Contributions**

826 AS initiated the study, KGJN generated the data, JF modeled terrestrial contributions
827 of isoGDGTs based on published information and the new Crenarchaeol data of the
828 modern peat dataset, which was contributed by GNI. All authors contributed to the
829 interpretation of the data and AS wrote the paper with input from all authors.

830

831 **9. Competing Interests**

832 The authors declare no competing interests

833

834 **10. Acknowledgments**

835 We thank the ACEX scientific party for collaborations over the past 16 years, the
836 International Ocean Discovery Program (IODP) for access to ACEX samples and data,



837 and the Dutch Research Council (NWO) for their continued support to IODP. We thank
838 Linda van Roij for analytical support.

839 This research was funded by European Research Council Consolidator Grant 771497
840 awarded to AS and the Netherlands Earth System Science Centre, funded through a
841 Gravitation Grant by the Netherlands Ministry of Education, Culture and Science and
842 NWO. GNI acknowledges a GCRF Royal Society Dorothy Hodgkin Fellowship.

843

844 **11. References**

- 845 Backman, J., Moran, K., McInroy, D. B., Mayer, L. A., and Expedition-302-Scientists:
846 Proceedings of the Integrated Ocean Drilling Program, 302, Integrated Ocean
847 Drilling Program Management International, Inc., Edinburgh, 2006.
- 848 Barke, J., Abels, H. A., Sangiorgi, F., Greenwood, D. R., Sweet, A. R., Donders, T.,
849 Reichart, G.-J., Lotter, A. F., and Brinkhuis, H.: Orbitally forced *Azolla* blooms
850 and Middle Eocene Arctic hydrology: Clues from palynology, *Geology*, 39, 427-
851 430, 10.1130/G31640.1, 2011.
- 852 Barke, J., van der Burgh, J., van Konijnenburg-van Cittert, J. H. A., Collinson, M. E.,
853 Pearce, M. A., Bujak, J., Heilmann-Clausen, C., Speelman, E. N., van Kempen, M.
854 M. L., Reichart, G.-J., Lotter, A. F., and Brinkhuis, H.: Coeval Eocene blooms of
855 the freshwater fern *Azolla* in and around Arctic and Nordic seas, *Palaeogeography,*
856 *Palaeoclimatology, Palaeoecology*, 337-338, 108-119,
857 <https://doi.org/10.1016/j.palaeo.2012.04.002>, 2012.
- 858 Baxter, A. J., Hopmans, E. C., Russell, J. M., and Sinninghe Damsté, J. S.: Bacterial
859 GMGTs in East African lake sediments: Their potential as palaeotemperature
860 indicators, *Geochim Cosmochim Acta*, 259, 155-169,
861 <https://doi.org/10.1016/j.gca.2019.05.039>, 2019.
- 862 Berry, E. W.: A Possible Explanation of Upper Eocene Climates, *Proceedings of the*
863 *American Philosophical Society*, 61, 1-14, 1922.
- 864 Besseling, M. A., Hopmans, E. C., Bale, N. J., Schouten, S., Damsté, J. S. S., and
865 Villanueva, L.: The absence of intact polar lipid-derived GDGTs in marine waters
866 dominated by Marine Group II: Implications for lipid biosynthesis in Archaea,
867 *Scientific Reports*, 10, 294, 10.1038/s41598-019-57035-0, 2020.
- 868 Bijl, P. K., Schouten, S., Sluijs, A., Reichart, G.-J., Zachos, J. C., and Brinkhuis, H.:
869 Early Palaeogene temperature evolution of the southwest Pacific Ocean, *Nature*,
870 461, 776-779, 2009.
- 871 Bijl, P. K., Bendle, J. A. P., Bohaty, S. M., Pross, J., Schouten, S., Tauxe, L., Stickley,
872 C. E., McKay, R. M., Rohl, U., Olney, M., Sluijs, A., Escutia, C., Brinkhuis, H.,
873 and the Expedition 318 Scientists: Eocene cooling linked to early flow across the
874 Tasmanian Gateway, *Proceedings of the National Academy of Sciences*, 110,
875 9645-9650, 10.1073/pnas.1220872110, 2013.
- 876 Blaga, C. I., Reichart, G.-J., Heiri, O., and Sinninghe Damsté, J. S.: Tetraether
877 membrane lipid distributions in water-column particulate matter and sediments: a



- 878 study of 47 European lakes along a north–south transect, *Journal of*
879 *Paleolimnology*, 41, 523–540, 10.1007/s10933-008-9242-2, 2009.
- 880 Brinkhuis, H., Schouten, S., Collinson, M. E., Sluijs, A., Sinninghe Damsté, J. S.,
881 Dickens, G. R., Huber, M., Cronin, T. M., Onodera, J., Takahashi, K., Bujak, J. P.,
882 Stein, R., van der Burgh, J., Eldrett, J. S., Harding, I. C., Lotter, A. F., Sangiorgi,
883 F., van Konijnenburg-van Cittert, H., de Leeuw, J. W., Matthiessen, J., Backman,
884 J., Moran, K., and the Expedition 302 Scientists: Episodic fresh surface waters in
885 the Eocene Arctic Ocean, *Nature*, 441, 606–609, 2006.
- 886 Carton, J. A., Ding, Y., and Arrigo, K. R.: The seasonal cycle of the Arctic Ocean under
887 climate change, *Geophysical Research Letters*, 42, 7681–7686,
888 doi:10.1002/2015GL064514, 2015.
- 889 Chepurin, G. A., and Carton, J. A.: Subarctic and Arctic sea surface temperature and its
890 relation to ocean heat content 1982–2010, *Journal of Geophysical Research: Oceans*,
891 117, doi:10.1029/2011JC007770, 2012.
- 892 Coolen, M. J. L., Abbas, B., Bleijswijk, J. v., Hopmans, E. C., Kuypers, M. M. M.,
893 Wakeham, S. G., and Damsté, J. S. S.: Putative ammonia-oxidizing Crenarchaeota
894 in suboxic waters of the Black Sea: a basin-wide ecological study using 16S
895 ribosomal and functional genes and membrane lipids, *Environ Microbiol*, 9, 1001–
896 1016, 2007.
- 897 Cramwinckel, M. J., Huber, M., Kocken, I. J., Agnini, C., Bijl, P. K., Bohaty, S. M.,
898 Frieling, J., Goldner, A., Hilgen, F. J., Kip, E. L., Peterse, F., van der Ploeg, R.,
899 Röhl, U., Schouten, S., and Sluijs, A.: Synchronous tropical and polar temperature
900 evolution in the Eocene, *Nature*, 559, 382–386, 10.1038/s41586-018-0272-2, 2018.
- 901 Cui, Y., Kump, L. R., Ridgwell, A. J., Charles, A. J., Junium, C. K., Diefendorf, A. F.,
902 Freeman, K. H., Urban, N. M., and Harding, I. C.: Slow release of fossil carbon
903 during the Palaeocene–Eocene Thermal Maximum, *Nature Geoscience*, 4, 481–485,
904 2011.
- 905 Dawson, M. R., West, R. M., Langston Jr, W., and Hutchison, J. H.: Paleogene
906 terrestrial vertebrates: Northernmost occurrence, Ellesmere Island, Canada,
907 *Science*, 192, 781–782, 1976.
- 908 De Jonge, C., Hopmans, E. C., Zell, C. I., Kim, J.-H., Schouten, S., and Sinninghe
909 Damsté, J. S.: Occurrence and abundance of 6-methyl branched glycerol dialkyl
910 glycerol tetraethers in soils: Implications for palaeoclimate reconstruction,
911 *Geochim Cosmochim Acta*, 141, 97–112, <https://doi.org/10.1016/j.gca.2014.06.013>,
912 2014.
- 913 De Jonge, C., Radujković, D., Sigurdsson, B. D., Weedon, J. T., Janssens, I., and
914 Peterse, F.: Lipid biomarker temperature proxy responds to abrupt shift in the
915 bacterial community composition in geothermally heated soils, *Org Geochem*, 137,
916 103897, <https://doi.org/10.1016/j.orggeochem.2019.07.006>, 2019.
- 917 De Rosa, M., Esposito, E., Gambacorta, A., Nicolaus, B., and Bu'Lock, J. D.: Effects
918 of temperature on ether lipid composition of *Caldariella acidophila*,
919 *Phytochemistry*, 19, 827–831, [https://doi.org/10.1016/0031-9422\(80\)85120-X](https://doi.org/10.1016/0031-9422(80)85120-X),
920 1980.
- 921 Dearing Crampton-Flood, E., Peterse, F., Munsterman, D., and Sinninghe Damsté, J.
922 S.: Using tetraether lipids archived in North Sea Basin sediments to extract North
923 Western European Pliocene continental air temperatures, *Earth and Planetary*
924 *Science Letters*, 490, 193–205, <https://doi.org/10.1016/j.epsl.2018.03.030>, 2018.
- 925 Dong, L., Li, Z., and Jia, G.: Archaeal ammonia oxidation plays a part in late
926 Quaternary nitrogen cycling in the South China Sea, *Earth and Planetary Science*
927 *Letters*, 509, 38–46, <https://doi.org/10.1016/j.epsl.2018.12.023>, 2019.



- 928 Douglas, P. M. J., Affek, H. P., Ivany, L. C., Houben, A. J. P., Sijp, W. P., Sluijs, A.,
929 Schouten, S., and Pagani, M.: Pronounced zonal heterogeneity in Eocene southern
930 high-latitude sea surface temperatures, *Proceedings of the National Academy of*
931 *Sciences of the United States of America*, 111, 6582-6587, 2014.
- 932 Eberle, J. J., and Greenwood, D. R.: Life at the top of the greenhouse Eocene world—
933 A review of the Eocene flora and vertebrate fauna from Canada's High Arctic,
934 *GSA Bulletin*, 124, 3-23, 10.1130/B30571.1, 2012.
- 935 Elling, F. J., Könneke, M., Lipp, J. S., Becker, K. W., Gagen, E. J., and Hinrichs, K.-
936 U.: Effects of growth phase on the membrane lipid composition of the
937 thaumarchaeon *Nitrosopumilus maritimus* and their implications for archaeal lipid
938 distributions in the marine environment, *Geochim Cosmochim Acta*, 141, 579-597,
939 <https://doi.org/10.1016/j.gca.2014.07.005>, 2014.
- 940 Elling, F. J., Könneke, M., Mußmann, M., Greve, A., and Hinrichs, K.-U.: Influence of
941 temperature, pH, and salinity on membrane lipid composition and TEX₈₆ of
942 marine planktonic thaumarchaeal isolates, *Geochim Cosmochim Acta*, 171, 238-255,
943 <https://doi.org/10.1016/j.gca.2015.09.004>, 2015.
- 944 Estes, R., and Hutchinson, J. H.: Eocene Lower Vertebrates from Ellesmere Island,
945 Canadian Arctic Archipelago, *Palaeogeography, Palaeoclimatology,*
946 *Palaeoecology*, 30, 325-347, 1980.
- 947 Evans, D., Sagoo, N., Renema, W., Cotton, L. J., Müller, W., Todd, J. A., Saraswati, P.
948 K., Stassen, P., Ziegler, M., Pearson, P. N., Valdes, P. J., and Affek, H. P.: Eocene
949 greenhouse climate revealed by coupled clumped isotope-Mg/Ca thermometry,
950 *Proceedings of the National Academy of Sciences*, 115, 1174-1179,
951 10.1073/pnas.1714744115, 2018.
- 952 Frieling, J., Iakovleva, A. I., Reichart, G. J., Aleksandrova, G. N., Gribidenko, Z. N.,
953 Schouten, S., and Sluijs, A.: Paleocene-Eocene warming and biotic response in the
954 epicontinental West Siberian Sea, *Geology*, 42, 767-770, 2014.
- 955 Frieling, J., Gebhardt, H., Huber, M., Adekeye, O. A., Akande, S. O., Reichart, G.-J.,
956 Middelburg, J. J., Schouten, S., and Sluijs, A.: Extreme warmth and heat-stressed
957 plankton in the tropics during the Paleocene-Eocene Thermal Maximum, *Science*
958 *Advances*, 3, e1600891, 10.1126/sciadv.1600891, 2017.
- 959 Frieling, J., and Sluijs, A.: Towards quantitative environmental reconstructions from
960 ancient non-analogue microfossil assemblages: Ecological preferences of
961 Paleocene – Eocene dinoflagellates, *Earth-Science Reviews*, 185, 956-973,
962 <https://doi.org/10.1016/j.earscirev.2018.08.014>, 2018.
- 963 Greenwood, D. R., and Wing, S. L.: Eocene continental climates and latitudinal
964 temperature gradients, *Geology*, 23, 1044-1048, 1995.
- 965 Greenwood, D. R., Basinger, J. F., and Smith, R. Y.: How wet was the Arctic Eocene
966 rain forest? Estimates of precipitation from Paleogene Arctic macrofloras,
967 *Geology*, 38, 15-18, 10.1130/G30218.1, 2010.
- 968 Harding, I. C., Charles, A. J., Marshall, J. E. A., Pälike, H., Roberts, A. P., Wilson, P.
969 A., Jarvis, E., Thorne, R., Morris, E., Moremon, R., Pearce, R. B., and Akbari, S.:
970 Sea-level and salinity fluctuations during the Paleocene-Eocene thermal maximum
971 in Arctic Spitsbergen, *Earth and Planetary Science Letters*, 303, 97-107, 2011.
- 972 Heer, O.: *Flora fossilis Arctica, Kongliga Svenska Vetenskaps Akademiens*
973 *Handlingar*, 4, Stockholm, Sweden, 41 pp., 1869.
- 974 Ho, S. L., Mollenhauer, G., Fietz, S., Martínez-García, A., Lamy, F., Rueda, G.,
975 Schipper, K., Méheust, M., Rosell-Melé, A., Stein, R., and Tiedemann, R.:
976 Appraisal of TEX₈₆ and TEX_{86L} thermometries in subpolar and polar regions,



- 977 Geochim Cosmochim Ac, 131, 213-226,
978 <https://doi.org/10.1016/j.gca.2014.01.001>, 2014.
- 979 Ho, S. L., and Laepple, T.: Flat meridional temperature gradient in the early Eocene in
980 the subsurface rather than surface ocean, *Nature Geoscience*, 9, 606-610,
981 10.1038/ngeo2763.<http://www.nature.com/ngeo/journal/v9/n8/abs/ngeo2763.html>
982 #supplementary-information, 2016.
- 983 Hollis, C. J., Dunkley Jones, T., Anagnostou, E., Bijl, P. K., Cramwinckel, M. J., Cui,
984 Y., Dickens, G. R., Edgar, K. M., Eley, Y., Evans, D., Foster, G. L., Frieling, J.,
985 Inglis, G. N., Kennedy, E. M., Kozdon, R., Lauretano, V., Lear, C. H., Littler, K.,
986 Lourens, L., Meckler, A. N., Naafs, B. D. A., Pälike, H., Pancost, R. D., Pearson,
987 P. N., Röhl, U., Royer, D. L., Salzmann, U., Schubert, B. A., Seebeck, H., Sluijs,
988 A., Speijer, R. P., Stassen, P., Tierney, J., Tripathi, A., Wade, B., Westerhold, T.,
989 Witkowski, C., Zachos, J. C., Zhang, Y. G., Huber, M., and Lunt, D. J.: The
990 DeepMIP contribution to PMIP4: methodologies for selection, compilation and
991 analysis of latest Paleocene and early Eocene climate proxy data, incorporating
992 version 0.1 of the DeepMIP database, *Geosci. Model Dev.*, 12, 3149-3206,
993 10.5194/gmd-12-3149-2019, 2019.
- 994 Hopmans, E. C., Schouten, S., Pancost, R. D., Meer, M. T. J. v. d., and Damsté, J. S.
995 S.: Analysis of intact tetraether lipids in archaeal cell material and sediments by
996 high performance liquid chromatography/atmospheric pressure chemical
997 ionization mass spectrometry, *Rapid Communications in Mass Spectrometry*, 14,
998 585-589, 2000.
- 999 Hopmans, E. C., Weijers, J. W. H., Schefuß, E., Herfort, L., Sinninghe Damsté, J. S.,
1000 and Schouten, S.: A novel proxy for terrestrial organic matter in sediments based
1001 on branched and isoprenoid tetraether lipids, *Earth and Planetary Science Letters*,
1002 224, 107-116, 2004.
- 1003 Hopmans, E. C., Schouten, S., and Sinninghe Damsté, J. S.: The effect of improved
1004 chromatography on GDGT-based palaeoproxies, *Org Geochem*, 93, 1-6,
1005 <https://doi.org/10.1016/j.orggeochem.2015.12.006>, 2016.
- 1006 Hurley, S. J., Elling, F. J., Könneke, M., Buchwald, C., Wankel, S. D., Santoro, A. E.,
1007 Lipp, J. S., Hinrichs, K.-U., and Pearson, A.: Influence of ammonia oxidation rate
1008 on thaumarchaeal lipid composition and the TEX₈₆ temperature proxy, *Proceedings*
1009 *of the National Academy of Sciences*, 113, 7762-7767, 10.1073/pnas.1518534113,
1010 2016.
- 1011 Inglis, G. N., Farnsworth, A., Lunt, D., Foster, G. L., Hollis, C. J., Pagani, M., Jardine,
1012 P. E., Pearson, P. N., Markwick, P., Galsworthy, A. M. J., Raynham, L., Taylor,
1013 K. W. R., and Pancost, R. D.: Descent toward the Icehouse: Eocene sea surface
1014 cooling inferred from GDGT distributions, *Paleoceanography*, 30, 1000-1020,
1015 10.1002/2014PA002723, 2015.
- 1016 Inglis, G. N., Farnsworth, A., Collinson, M. E., Carmichael, M. J., Naafs, B. D. A.,
1017 Lunt, D. J., Valdes, P. J., and Pancost, R. D.: Terrestrial environmental change
1018 across the onset of the PETM and the associated impact on biomarker proxies: A
1019 cautionary tale, *Global and Planetary Change*, 181, 102991,
1020 <https://doi.org/10.1016/j.gloplacha.2019.102991>, 2019.
- 1021 Karner, M. B., DeLong, E. F., and Karl, D. M.: Archaeal dominance in the mesopelagic
1022 zone of the Pacific Ocean, *Nature*, 409, 507-510, 10.1038/35054051, 2001.
- 1023 Kim, J.-H., Schouten, S., Hopmans, E. C., Donner, B., and Sinninghe Damsté, J. S.:
1024 Global sediment core-top calibration of the TEX₈₆ paleothermometer in the ocean,
1025 *Geochim Cosmochim Ac*, 72, 1154-1173, 2008.



- 1026 Kim, J.-H., van der Meer, J., Schouten, S., Helmke, P., Willmott, V., Sangiorgi, F.,
1027 Koç, N., Hopmans, E. C., and Sinninghe Damsté, J. S.: New indices and
1028 calibrations derived from the distribution of crenarchaeal isoprenoid tetraether
1029 lipids: Implications for past sea surface temperature reconstructions, *Geochim*
1030 *Cosmochim Ac*, 74, 4639-4654, 2010.
- 1031 Kim, J.-H., Schouten, S., Rodrigo-Gámiz, M., Rampen, S., Marino, G., Huguet, C.,
1032 Helmke, P., Buscail, R., Hopmans, E. C., Pross, J., Sangiorgi, F., Middelburg, J.
1033 B. M., and Sinninghe Damsté, J. S.: Influence of deep-water derived isoprenoid
1034 tetraether lipids on the paleothermometer in the Mediterranean Sea, *Geochim*
1035 *Cosmochim Ac*, 150, 125-141, <http://dx.doi.org/10.1016/j.gca.2014.11.017>, 2015.
- 1036 Kirkels, F. M. S. A., Ponton, C., Galy, V., West, A. J., Feakins, S. J., and Peterse, F.:
1037 From Andes to Amazon: Assessing Branched Tetraether Lipids as Tracers for Soil
1038 Organic Carbon in the Madre de Dios River System, *Journal of Geophysical*
1039 *Research: Biogeosciences*, 125, e2019JG005270, 10.1029/2019jg005270, 2020.
- 1040 Knies, J., Mann, U., Popp, B. N., Stein, R., and Brumsack, H.-J.: Surface water
1041 productivity and paleoceanographic implications in the Cenozoic Arctic Ocean,
1042 *Paleoceanography*, 23, PA1S16, 10.1029/2007pa001455, 2008.
- 1043 Könneke, M., Bernhard, A. E., de la Torre, J. R., Walker, C. B., Waterbury, J. B., and
1044 Stahl, D. A.: Isolation of an autotrophic ammonia-oxidizing marine archaeon,
1045 *Nature*, 437, 543-546, 10.1038/nature03911, 2005.
- 1046 Krishnan, S., Pagani, M., Huber, M., and Sluijs, A.: High latitude hydrological changes
1047 during the Eocene Thermal Maximum 2, *Earth and Planetary Science Letters*, 404,
1048 167-177, 2014.
- 1049 Liu, X.-L., Summons, R. E., and Hinrichs, K.-U.: Extending the known range of
1050 glycerol ether lipids in the environment: structural assignments based on tandem
1051 mass spectral fragmentation patterns, *Rapid Communications in Mass*
1052 *Spectrometry*, 26, 2295-2302, 10.1002/rcm.6355, 2012.
- 1053 Liu, Z., Pagani, M., Zinniker, D., DeConto, R., Huber, M., Brinkhuis, H., Shah, S. R.,
1054 Leckie, R. M., and Pearson, A.: Global Cooling During the Eocene-Oligocene
1055 Climate Transition, *Science*, 323, 1187-1190, 10.1126/science.1166368, 2009.
- 1056 Lunt, D. J., Jones, T. D., Heinemann, M., Huber, M., LeGrande, A., Winguth, A.,
1057 Loptson, C., Marotzke, J., Roberts, C. D., Tindall, J., Valdes, P., and Winguth, C.:
1058 A model–data comparison for a multi-model ensemble of early Eocene
1059 atmosphere–ocean simulations: EoMIP, *Climate of the Past*, 8, 1717-1736, 2012.
- 1060 März, C., Schnetger, B., and Brumsack, H. J.: Paleoenvironmental implications of
1061 Cenozoic sediments from the central Arctic Ocean (IODP Expedition 302) using
1062 inorganic geochemistry, *Paleoceanography*, 25, PA3206, 10.1029/2009pa001860,
1063 2010.
- 1064 Menzel, D., Hopmans, E. C., Schouten, S., and Sinninghe Damsté, J. S.: Membrane
1065 tetraether lipids of planktonic Crenarchaeota in Pliocene sapropels of the eastern
1066 Mediterranean Sea, *Palaeogeography, Palaeoclimatology, Palaeoecology*, 239, 1-
1067 15, 2006.
- 1068 Mollenhauer, G., Basse, A., Kim, J.-H., Sinninghe Damsté, J. S., and Fischer, G.: A
1069 four-year record of UK' 37- and TEX86-derived sea surface temperature
1070 estimates from sinking particles in the filamentous upwelling region off Cape
1071 Blanc, Mauritania, *Deep Sea Research Part I: Oceanographic Research Papers*, 97,
1072 67-79, <https://doi.org/10.1016/j.dsr.2014.11.015>, 2015.
- 1073 Morales, C., Rogov, M., Wierzbowski, H., Ershova, V., Suan, G., Adatte, T., Föllmi,
1074 K. B., Tegelaar, E., Reichart, G.-J., de Lange, G. J., Middelburg, J. J., and van de



- 1075 Schootbrugge, B.: Glendonites track methane seepage in Mesozoic polar seas,
1076 *Geology*, 45, 503-506, 10.1130/g38967.1, 2017.
- 1077 Naafs, B. D. A., Inglis, G. N., Zheng, Y., Amesbury, M. J., Biester, H., Bindler, R.,
1078 Blewett, J., Burrows, M. A., del Castillo Torres, D., Chambers, F. M., Cohen, A.
1079 D., Evershed, R. P., Feakins, S. J., Gałka, M., Gallego-Sala, A., Gandois, L., Gray,
1080 D. M., Hatcher, P. G., Honorio Coronado, E. N., Hughes, P. D. M., Huguet, A.,
1081 Könönen, M., Laggoun-Défarge, F., Lähteenoja, O., Lamentowicz, M., Marchant,
1082 R., McClymont, E., Pontevedra-Pombal, X., Ponton, C., Pourmand, A., Rizzuti, A.
1083 M., Rochefort, L., Schellekens, J., De Vleeschouwer, F., and Pancost, R. D.:
1084 Introducing global peat-specific temperature and pH calibrations based on
1085 brGDGT bacterial lipids, *Geochim Cosmochim Acta*, 208, 285-301,
1086 <https://doi.org/10.1016/j.gca.2017.01.038>, 2017.
- 1087 Naafs, B. D. A., McCormick, D., Inglis, G. N., and Pancost, R. D.: Archaeal and
1088 bacterial H-GDGTs are abundant in peat and their relative abundance is positively
1089 correlated with temperature, *Geochim Cosmochim Acta*, 227, 156-170,
1090 <https://doi.org/10.1016/j.gca.2018.02.025>, 2018a.
- 1091 Naafs, B. D. A., Rohrsen, M., Inglis, G. N., Lähteenoja, O., Feakins, S. J., Collinson,
1092 M. E., Kennedy, E. M., Singh, P. K., Singh, M. P., Lunt, D. J., and Pancost, R. D.:
1093 High temperatures in the terrestrial mid-latitudes during the early Palaeogene,
1094 *Nature Geoscience*, 11, 766-771, 10.1038/s41561-018-0199-0, 2018b.
- 1095 O'Brien, C. L., Robinson, S. A., Pancost, R. D., Sinninghe Damsté, J. S., Schouten, S.,
1096 Lunt, D. J., Alsenz, H., Bornemann, A., Bottini, C., Brassell, S. C., Farnsworth, A.,
1097 Forster, A., Huber, B. T., Inglis, G. N., Jenkyns, H. C., Linnert, C., Littler, K.,
1098 Markwick, P., McAnena, A., Mutterlose, J., Naafs, B. D. A., Püttmann, W., Sluijs,
1099 A., van Helmond, N. A. G. M., Vellekoop, J., Wagner, T., and Wrobel, N. E.:
1100 Cretaceous sea-surface temperature evolution: Constraints from TEX86 and
1101 planktonic foraminiferal oxygen isotopes, *Earth-Science Reviews*, 172, 224-247,
1102 <https://doi.org/10.1016/j.earscirev.2017.07.012>, 2017.
- 1103 O'Regan, M., Moran, K., Sangiorgi, F., Brinkhuis, H., Backman, J., Jakobsson, M.,
1104 Stickley, C. E., Koc, N., Brumsack, H., Willard, D., Pockalny, R., and Skelton, A.:
1105 Mid-Cenozoic Tectonic and Palaeoenvironmental setting of the Central Arctic
1106 Ocean, *Paleoceanography*, 23, PA1S20, doi:10.1029/2007PA001559, 2008.
- 1107 Pagani, M., Pedentchouk, N., Huber, M., Sluijs, A., Schouten, S., Brinkhuis, H.,
1108 Sinninghe Damsté, J. S., Dickens, G. R., and Expedition 302 Scientists, T.: Arctic
1109 hydrology during global warming at the Palaeocene-Eocene thermal maximum,
1110 *Nature*, 442, 671-675, 2006.
- 1111 Park, E., Hefter, J., Fischer, G., Iversen, M. H., Ramondenc, S., Nöthig, E. M., and
1112 Mollenhauer, G.: Seasonality of archaeal lipid flux and GDGT-based thermometry
1113 in sinking particles of high-latitude oceans: Fram Strait (79°N) and Antarctic Polar
1114 Front (50°S), *Biogeosciences*, 16, 2247-2268, 10.5194/bg-16-2247-2019, 2019.
- 1115 Pierrehumbert, R. T.: The hydrologic cycle in deep-time climate problems, *Nature*, 419,
1116 191-198, 2002.
- 1117 Pitcher, A., Hopmans, E. C., Mosier, A. C., Park, S.-J., Rhee, S.-K., Francis, C. A.,
1118 Schouten, S., and Sinninghe Damsté, J. S.: Core and Intact Polar Glycerol
1119 Dibiphytanyl Glycerol Tetraether Lipids of Ammonia-Oxidizing Archaea
1120 Enriched from Marine and Estuarine Sediments, *Applied and Environmental
1121 Microbiology*, 77, 3468-3477, 10.1128/aem.02758-10, 2011a.
- 1122 Pitcher, A., Wuchter, C., Siedenberg, K., Schouten, S., and Sinninghe Damsté, J. S.:
1123 Crenarchaeol tracks winter blooms of ammonia-oxidizing Thaumarchaeota in the



- 1124 coastal North Sea, *Limnol Oceanogr*, 56, 2308-2318, 10.4319/lo.2011.56.6.2308,
1125 2011b.
- 1126 Qin, W., Amin, S. A., Martens-Habbena, W., Walker, C. B., Urakawa, H., Devol, A.
1127 H., Ingalls, A. E., Moffett, J. W., Armbrust, E. V., and Stahl, D. A.: Marine
1128 ammonia-oxidizing archaeal isolates display obligate mixotrophy and wide
1129 ecotypic variation, *Proceedings of the National Academy of Sciences*, 111, 12504-
1130 12509, 10.1073/pnas.1324115111, 2014.
- 1131 Qin, W., Carlson, L. T., Armbrust, E. V., Devol, A. H., Moffett, J. W., Stahl, D. A., and
1132 Ingalls, A. E.: Confounding effects of oxygen and temperature on the TEX₈₆
1133 signature of marine Thaumarchaeota, *Proceedings of the National Academy of
1134 Sciences*, 112, 10979-10984, 10.1073/pnas.1501568112, 2015.
- 1135 Reichgelt, T., West, C. K., and Greenwood, D. R.: The relation between global palm
1136 distribution and climate, *Scientific Reports*, 8, 4721, 10.1038/s41598-018-23147-
1137 2, 2018.
- 1138 Richey, J. N., and Tierney, J. E.: GDGT and alkenone flux in the northern Gulf of
1139 Mexico: Implications for the TEX₈₆ and UK'37 paleothermometers,
1140 *Paleoceanography*, 31, 1547-1561, 10.1002/2016pa003032, 2016.
- 1141 Sangiorgi, F., van Soelen, E. E., Spofforth, D. J. A., Pälike, H., Stickley, C. E., St. John,
1142 K., Koç, N., Schouten, S., Sinninghe Damsté, J. S., and Brinkhuis, H.: Cyclicity in
1143 the middle Eocene central Arctic Ocean sediment record: Orbital forcing and
1144 environmental response, *Paleoceanography*, 23, n/a-n/a, 10.1029/2007PA001487,
1145 2008.
- 1146 Schouten, S., Hopmans, E. C., Schefuß, E., and Sinninghe Damsté, J. S.: Distributional
1147 variations in marine crenarchaeotal membrane lipids: a new tool for reconstructing
1148 ancient sea water temperatures?, *Earth and Planetary Science Letters*, 204, 265-
1149 274, 2002.
- 1150 Schouten, S., Hopmans, E. C., Forster, A., Breugel, Y. V., Kuypers, M. M. M., and
1151 Sinninghe Damsté, J. S.: Extremely high sea-surface temperatures at low latitudes
1152 during the middle Cretaceous as revealed by archaeal membrane lipids, *Geology*,
1153 31, 1069-1072, 2003.
- 1154 Schouten, S., Forster, A., Panoto, F. E., and Sinninghe Damsté, J. S.: Towards
1155 calibration of the TEX₈₆ palaeothermometer for tropical sea surface temperatures
1156 in ancient greenhouse worlds, *Org Geochem*, 38, 1537-1546, 2007a.
- 1157 Schouten, S., Woltering, M., Rijpstra, W. I. C., Sluijs, A., Brinkhuis, H., and Sinninghe
1158 Damsté, J. S.: The Paleocene-Eocene carbon isotope excursion in higher plant
1159 organic matter: Differential fractionation of angiosperms and conifers in the Arctic,
1160 *Earth and Planetary Science Letters*, 258, 581-592, 2007b.
- 1161 Schouten, S., Baas, M., Hopmans, E. C., and Sinninghe Damsté, J. S.: An unusual
1162 isoprenoid tetraether lipid in marine and lacustrine sediments, *Org Geochem*, 39,
1163 1033-1038, 2008.
- 1164 Schouten, S., Hopmans, E. C., Meer, J. v. d., Mets, A., Bard, E., Bianchi, T. S.,
1165 Diefendorf, A., Escala, M., Freeman, K. H., Furukawa, Y., Ingalls, C. H. a. A.,
1166 Ménot-Combes, G., Nederbragt, A. J., Oba, M., Pearson, A., Pearson, E. J., Rosell-
1167 Melé, A., Schaeffer, P., Shah, S. R., Shanahan, T. M., Smith, R. W., Smittenberg,
1168 R., Talbot, H. M., Uchida, M., Mooy, B. A. S. V., Yamamoto, M., Zhang, Z., and
1169 Sinninghe Damsté, J. S.: An interlaboratory study of TEX₈₆ and BIT analysis
1170 using high-performance liquid chromatography–mass spectrometry, *Geochemistry
1171 Geophysics Geosystems*, 10, Q03012, doi:03010.01029/02008GC002221, 2009.



- 1172 Schouten, S., Hopmans, E. C., and Sinninghe Damsté, J. S.: The organic geochemistry
1173 of glycerol dialkyl glycerol tetraether lipids: A review, *Org Geochem*, 54, 19-61,
1174 <http://dx.doi.org/10.1016/j.orggeochem.2012.09.006>, 2013.
- 1175 Schweitzer, H.-J.: Environment and climate in the early Tertiary of Spitsbergen,
1176 *Palaeogeography, Palaeoclimatology, Palaeoecology*, 30, 297-311, 1980.
- 1177 Seton, M., Müller, R. D., Zahirovic, S., Gaina, C., Torsvik, T., Shephard, G., Talsma,
1178 A., Gurnis, M., Turner, M., Maus, S., and Chandler, M.: Global continental and
1179 ocean basin reconstructions since 200Ma, *Earth-Science Reviews*, 113, 212-270,
1180 <https://doi.org/10.1016/j.earscirev.2012.03.002>, 2012.
- 1181 Shah, S. R., Mollenhauer, G., Ohkouchi, N., Eglinton, T. I., and Pearson, A.: Origins
1182 of archaeal tetraether lipids in sediments: Insights from radiocarbon analysis,
1183 *Geochim Cosmochim Acta*, 72, 4577-4594,
1184 <https://doi.org/10.1016/j.gca.2008.06.021>, 2008.
- 1185 Sinninghe Damsté, J. S., Wakeham, S. G., Kohnen, M. E. L., Hayes, J. M., and de
1186 Leeuw, J. W.: A 6,000-year sedimentary molecular record of chemocline
1187 excursions in the Black Sea, *Nature*, 362, 827 - 829, 1993.
- 1188 Sinninghe Damsté, J. S., Rijpstra, W. I. C., Hopmans, E. C., Weijers, J. W. H., Foessel,
1189 B. U., Overmann, J., and Dedysh, S. N.: 13,16-Dimethyl Octacosanedioic Acid
1190 (*iso*-Diabolic Acid), a Common Membrane-Spanning Lipid of Acidobacteria
1191 Subdivisions 1 and 3, *Applied and Environmental Microbiology*, 77, 4147-4154,
1192 [10.1128/aem.00466-11](https://doi.org/10.1128/aem.00466-11), 2011.
- 1193 Sinninghe Damsté, J. S.: Spatial heterogeneity of sources of branched tetraethers in
1194 shelf systems: The geochemistry of tetraethers in the Berau River delta
1195 (Kalimantan, Indonesia), *Geochim Cosmochim Acta*, 186, 13-31,
1196 <https://doi.org/10.1016/j.gca.2016.04.033>, 2016.
- 1197 Sinninghe Damsté, J. S., Rijpstra, W. I. C., Foessel, B. U., Huber, K. J., Overmann, J.,
1198 Nakagawa, S., Kim, J. J., Dunfield, P. F., Dedysh, S. N., and Villanueva, L.: An
1199 overview of the occurrence of ether- and ester-linked *iso*-diabolic acid membrane
1200 lipids in microbial cultures of the Acidobacteria: Implications for brGDGT
1201 paleoproxies for temperature and pH, *Org Geochem*, 124, 63-76,
1202 <https://doi.org/10.1016/j.orggeochem.2018.07.006>, 2018.
- 1203 Sluijs, A., Schouten, S., Pagani, M., Woltering, M., Brinkhuis, H., Sinninghe Damsté,
1204 J. S., Dickens, G. R., Huber, M., Reichart, G.-J., Stein, R., Matthiessen, J., Lourens,
1205 L. J., Pedentchouk, N., Backman, J., Moran, K., and The Expedition 302 Scientists:
1206 Subtropical Arctic Ocean temperatures during the Palaeocene/Eocene thermal
1207 maximum, *Nature*, 441, 610-613, 2006.
- 1208 Sluijs, A., Brinkhuis, H., Crouch, E. M., John, C. M., Handley, L., Munsterman, D.,
1209 Bohaty, S. M., Zachos, J. C., Reichart, G.-J., Schouten, S., Pancost, R. D.,
1210 Sinninghe Damsté, J. S., Welters, N. L. D., Lotter, A. F., and Dickens, G. R.:
1211 Eustatic variations during the Paleocene-Eocene greenhouse world,
1212 *Paleoceanography*, 23, PA4216, doi:10.1029/2008PA001615, 2008a.
- 1213 Sluijs, A., Röhl, U., Schouten, S., Brumsack, H.-J., Sangiorgi, F., Sinninghe Damsté, J.
1214 S., and Brinkhuis, H.: Arctic late Paleocene–early Eocene paleoenvironments with
1215 special emphasis on the Paleocene-Eocene thermal maximum (Lomonosov Ridge,
1216 Integrated Ocean Drilling Program Expedition 302), *Paleoceanography*, 23,
1217 PA1S11, doi:10.1029/2007PA001495, 2008b.
- 1218 Sluijs, A., Schouten, S., Donders, T. H., Schoon, P. L., Röhl, U., Reichart, G. J.,
1219 Sangiorgi, F., Kim, J.-H., Sinninghe Damsté, J. S., and Brinkhuis, H.: Warm and
1220 Wet Conditions in the Arctic Region during Eocene Thermal Maximum 2, *Nature*
1221 *Geoscience*, 2, 777-780, 2009.



- 1222 Sluijs, A., and Dickens, G. R.: Assessing offsets between the $\delta^{13}\text{C}$ of sedimentary
1223 components and the global exogenic carbon pool across Early Paleogene carbon
1224 cycle perturbations, *Global Biogeochemical Cycles*, 26, GB4005,
1225 doi:10.1029/2011GB004224, 2012.
- 1226 Sollich, M., Yoshinaga, M. Y., Häusler, S., Price, R. E., Hinrichs, K.-U., and Bühring,
1227 S. I.: Heat Stress Dictates Microbial Lipid Composition along a Thermal Gradient
1228 in Marine Sediments, *Frontiers in Microbiology*, 8, 10.3389/fmicb.2017.01550,
1229 2017.
- 1230 Speelman, E. N., Van Kempen, M. M. L., Barke, J., Brinkhuis, H., Reichart, G. J.,
1231 Smolders, A. J. P., Roelofs, J. G. M., Sangiorgi, F., De Leeuw, J. W., Lotter, A. F.,
1232 and Sinninghe Damsté, J. S.: The Eocene Arctic Azolla bloom: environmental
1233 conditions, productivity and carbon drawdown, *Geobiology*, 7, 155-170,
1234 10.1111/j.1472-4669.2009.00195.x, 2009.
- 1235 Speelman, E. N., Sewall, J. O., Noone, D., Huber, M., der Heydt, A. v., Damsté, J. S.,
1236 and Reichart, G.-J.: Modeling the influence of a reduced equator-to-pole sea
1237 surface temperature gradient on the distribution of water isotopes in the
1238 Early/Middle Eocene, *Earth and Planetary Science Letters*, 298, 57-65,
1239 <https://doi.org/10.1016/j.epsl.2010.07.026>, 2010.
- 1240 Spielhagen, R. F., and Tripathi, A.: Evidence from Svalbard for near-freezing
1241 temperatures and climate oscillations in the Arctic during the Paleocene and
1242 Eocene, *Palaeogeography, Palaeoclimatology, Palaeoecology*, 278, 48-56,
1243 <https://doi.org/10.1016/j.palaeo.2009.04.012>, 2009.
- 1244 Stein, R., Boucsein, B., and Meyer, H.: Anoxia and high primary production in the
1245 Paleogene central Arctic Ocean: First detailed records from Lomonosov Ridge,
1246 *Geophysical Research Letters*, 33, L18606, doi:10.1029/2006GL026776, 2006.
- 1247 Stein, R.: Upper Cretaceous/lower Tertiary black shales near the North Pole: Organic-
1248 carbon origin and source-rock potential, *Marine and Petroleum Geology*, 24, 67-
1249 73, 2007.
- 1250 Suan, G., Popescu, S.-M., Yoon, D., Baudin, F., Suc, J.-P., Schnyder, J., Labrousse, L.,
1251 Fauquette, S., Piepjohn, K., and Sobolev, N. N.: Subtropical climate conditions and
1252 mangrove growth in Arctic Siberia during the early Eocene, *Geology*, 45, 539-542,
1253 10.1130/g38547.1, 2017.
- 1254 Taylor, K. W. R., Huber, M., Hollis, C. J., Hernandez-Sanchez, M. T., and Pancost, R.
1255 D.: Re-evaluating modern and Palaeogene GDGT distributions: Implications for
1256 SST reconstructions, *Global and Planetary Change*, 108, 158-174,
1257 <http://dx.doi.org/10.1016/j.gloplacha.2013.06.011>, 2013.
- 1258 Teichert, B. M. A., and Luppold, F. W.: Glendonites from an Early Jurassic methane
1259 seep — Climate or methane indicators?, *Palaeogeography, Palaeoclimatology,*
1260 *Palaeoecology*, 390, 81-93, <https://doi.org/10.1016/j.palaeo.2013.03.001>, 2013.
- 1261 Tierney, J. E., and Tingley, M. P.: A Bayesian, spatially-varying calibration model for
1262 the TEX86 proxy, *Geochim Cosmochim Acta*, 127, 83-106,
1263 <http://dx.doi.org/10.1016/j.gca.2013.11.026>, 2014.
- 1264 Tierney, J. E., Sinninghe Damsté, J. S., Pancost, R. D., Sluijs, A., and Zachos, J. C.:
1265 Eocene temperature gradients, *Nature Geosci*, 10, 538-539, 10.1038/ngeo2997,
1266 2017.
- 1267 Torsvik, T. H., Van der Voo, R., Preeden, U., Mac Niocaill, C., Steinberger, B.,
1268 Doubrovine, P. V., van Hinsbergen, D. J. J., Domeier, M., Gaina, C., Tohver, E.,
1269 Meert, J. G., McCausland, P. J. A., and Cocks, L. R. M.: Phanerozoic polar wander,
1270 palaeogeography and dynamics, *Earth-Science Reviews*, 114, 325-368,
1271 <https://doi.org/10.1016/j.earscirev.2012.06.007>, 2012.



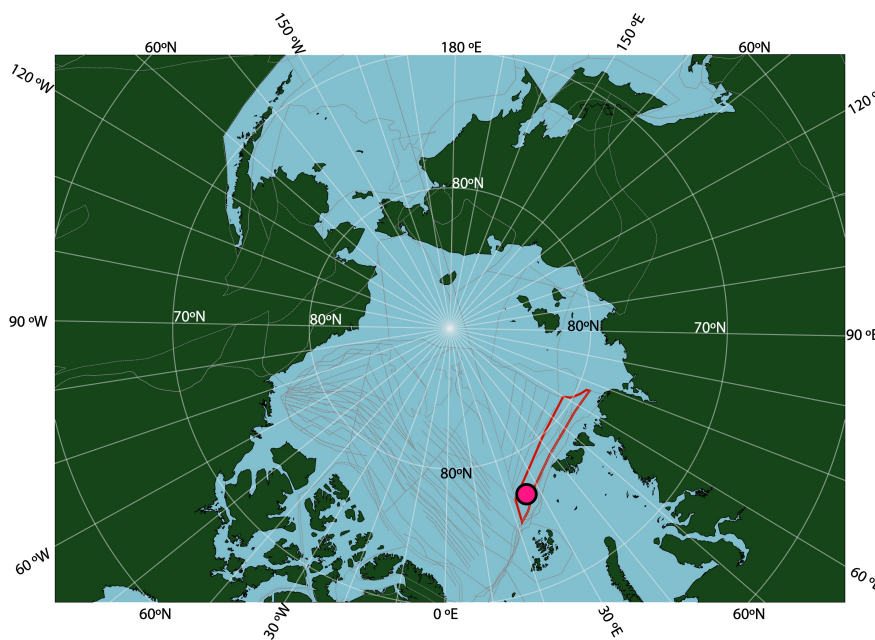
- 1272 Trommer, G., Siccha, M., van der Meer, M. T. J., Schouten, S., Sinninghe Damsté, J.
1273 S., Schulz, H., Hemleben, C., and Kucera, M.: Distribution of Crenarchaeota
1274 tetraether membrane lipids in surface sediments from the Red Sea, *Org Geochem*,
1275 40, 724-731, <https://doi.org/10.1016/j.orggeochem.2009.03.001>, 2009.
- 1276 Uhl, D., Traiser, C., Griesser, U., and Denk, T.: Fossil leaves as palaeoclimate proxies
1277 in the Palaeogene of Spitsbergen (Svalbard), *Acta Palaeobotanica*, 47, 89-107,
1278 2007.
- 1279 Van der Burgh, J.: Some palms in the Miocene of the lower Rhenish Plain, *Review of*
1280 *Palaeobotany and Palynology*, 40, 359-374, 1984.
- 1281 Van Hinsbergen, D. J. J., de Groot, L. V., van Schaik, S. J., Spakman, W., Bijl, P. K.,
1282 Sluijs, A., Langereis, C. G., and Brinkhuis, H.: A Paleolatitude Calculator for
1283 Paleoclimate Studies, *PLOS ONE*, 10, e0126946, [10.1371/journal.pone.0126946](https://doi.org/10.1371/journal.pone.0126946),
1284 2015.
- 1285 Waddell, L. M., and Moore, T. C.: Salinity of the Eocene Arctic Ocean from Oxygen
1286 Isotope Analysis of Fish Bone Carbonate, *Paleoceanography*, 23, PA1S12,
1287 [doi:10.1029/2007PA001451](https://doi.org/10.1029/2007PA001451), 2008.
- 1288 Wakeham, S. G., Amann, R., Freeman, K. H., Hopmans, E. C., Jörgensen, B. B.,
1289 Putnam, I. F., Schouten, S., Sinninghe Damsté, J. S., Talbot, H. M., and Woeikén,
1290 D.: Microbial ecology of the stratified water column of the Black Sea as revealed
1291 by a comprehensive biomarker study, *Org Geochem*, 38, 2070-2097, 2007.
- 1292 Weijers, J. W. H., Schouten, S., Spaargaren, O. C., and Sinninghe Damsté, J. S.:
1293 Occurrence and distribution of tetraether membrane lipids in soils: Implications for
1294 the use of the TEX86 proxy and the BIT index, *Org Geochem*, 37, 1680-1693,
1295 2006.
- 1296 Weijers, J. W. H., Schouten, S., Sluijs, A., Brinkhuis, H., and Sinninghe Damsté, J. S.:
1297 Warm arctic continents during the Palaeocene-Eocene thermal maximum, *Earth*
1298 *and Planetary Science Letters*, 261, 230-238, 2007.
- 1299 Weijers, J. W. H., Lim, K. L. H., Aquilina, A., Sinninghe Damsté, J. S., and Pancost,
1300 R. D.: Biogeochemical controls on glycerol dialkyl glycerol tetraether lipid
1301 distributions in sediments characterized by diffusive methane flux, *Geochemistry*,
1302 *Geophysics, Geosystems*, 12, [doi:10.1029/2011GC003724](https://doi.org/10.1029/2011GC003724), 2011.
- 1303 Weller, P., and Stein, R.: Paleogene biomarker records from the central Arctic Ocean
1304 (Integrated Ocean Drilling Program Expedition 302): Organic carbon sources,
1305 anoxia, and sea surface temperature, *Paleoceanography*, 23,
1306 [doi:10.1029/2007PA001472](https://doi.org/10.1029/2007PA001472), 2008.
- 1307 Willard, D. A., Donders, T. H., Reichgelt, T., Greenwood, D. R., Sangiorgi, F., Peterse,
1308 F., Nierop, K. G. J., Frieling, J., Schouten, S., and Sluijs, A.: Arctic vegetation,
1309 temperature, and hydrology during Early Eocene transient global warming events,
1310 *Global and Planetary Change*, 178, 139-152,
1311 <https://doi.org/10.1016/j.gloplacha.2019.04.012>, 2019.
- 1312 Wuchter, C., Schouten, S., Coolen, M. J. L., and Sinninghe Damsté, J. S.: Temperature-
1313 dependent variation in the distribution of tetraether membrane lipids of marine
1314 Crenarchaeota: Implications for TEX86 paleothermometry, *Paleoceanography*, 19,
1315 PA402, 2004.
- 1316 Wuchter, C., Schouten, S., Wakeham, S. G., and Sinninghe Damsté, J. S.: Temporal
1317 and spatial variation in tetraether membrane lipids of marine Crenarchaeota in
1318 particulate organic matter: Implications for TEX86 paleothermometry,
1319 *Paleoceanography*, 20, [doi:10.1029/2004PA001110](https://doi.org/10.1029/2004PA001110), 2005.
- 1320 Wuchter, C., Abbas, B., Coolen, M. J. L., Herfort, L., van Bleijswijk, J., Timmers, P.,
1321 Strous, M., Teira, E., Herndl, G. J., Middelburg, J. J., Schouten, S., and Damsté, J.



- 1322 S. S.: Archaeal nitrification in the ocean, *Proceedings of the National Academy of*
1323 *Sciences of the United States of America*, 103, 12317-12322,
1324 10.1073/pnas.0600756103, 2006a.
- 1325 Wuchter, C., Schouten, S., Wakeham, S. G., and Sinninghe Damsté, J. S.: Archaeal
1326 tetraether membrane lipid fluxes in the northeastern Pacific and the Arabian Sea:
1327 Implications for TEX86 paleothermometry, *Paleoceanography*, 21, PA4208,
1328 2006b.
- 1329 Xie, S., Liu, X.-L., Schubotz, F., Wakeham, S. G., and Hinrichs, K.-U.: Distribution of
1330 glycerol ether lipids in the oxygen minimum zone of the Eastern Tropical North
1331 Pacific Ocean, *Org Geochem*, 71, 60-71,
1332 <https://doi.org/10.1016/j.orggeochem.2014.04.006>, 2014.
- 1333 Yamamoto, M., Shimamoto, A., Fukuhara, T., Tanaka, Y., and Ishizaka, J.: Glycerol
1334 dialkyl glycerol tetraethers and TEX86 index in sinking particles in the western
1335 North Pacific, *Org Geochem*, 53, 52-62,
1336 <https://doi.org/10.1016/j.orggeochem.2012.04.010>, 2012.
- 1337 Zeng, Z., Liu, X.-L., Farley, K. R., Wei, J. H., Metcalf, W. W., Summons, R. E., and
1338 Welander, P. V.: GDGT cyclization proteins identify the dominant archaeal
1339 sources of tetraether lipids in the ocean, *Proceedings of the National Academy of*
1340 *Sciences*, 116, 22505-22511, 10.1073/pnas.1909306116, 2019.
- 1341 Zhang, Y. G., Zhang, C. L., Liu, X.-L., Li, L., Hinrichs, K.-U., and Noakes, J. E.:
1342 Methane Index: A tetraether archaeal lipid biomarker indicator for detecting the
1343 instability of marine gas hydrates, *Earth and Planetary Science Letters*, 307, 525-
1344 534, <https://doi.org/10.1016/j.epsl.2011.05.031>, 2011.
- 1345 Zhang, Y. G., Pagani, M., and Wang, Z.: Ring Index: A new strategy to evaluate the
1346 integrity of TEX86 paleothermometry, *Paleoceanography*, 31, 220-232,
1347 doi:10.1002/2015PA002848, 2016.
- 1348 Zhang, Y. G., and Liu, X.: Export Depth of the TEX86 Signal, *Paleoceanography and*
1349 *Paleoclimatology*, 33, 666-671, 10.1029/2018pa003337, 2018.
- 1350 Zhu, G. Y., Chen, J., Liu, J., Brunzelle, J. S., Huang, B., Wakeham, N., Terzyan, S., Li,
1351 X. M., Rao, Z., Li, G. P., and Zhang, X. J. C.: Structure of the APPL1 BAR-PH
1352 domain and characterization of its interaction with Rab5, *Embo J*, 26, 3484-3493,
1353 2007.
- 1354 Zhu, J., Poulsen, C. J., and Tierney, J. E.: Simulation of Eocene extreme warmth and
1355 high climate sensitivity through cloud feedbacks, *Science Advances*, 5, eaax1874,
1356 10.1126/sciadv.aax1874, 2019.
- 1357



1358 **Figure 1.** Location of ACEX Hole 4A within a paleogeographic reconstruction of the
1359 Arctic region at the time of the PETM. Reconstruction made using gplates, using the
1360 tectonic reconstruction of Seton et al. (2012, red shape is Lomonosov Ridge in this
1361 reconstruction) using the paleomagnetic reference frame of Torsvik et al., (2012), and
1362 modern coastlines.
1363



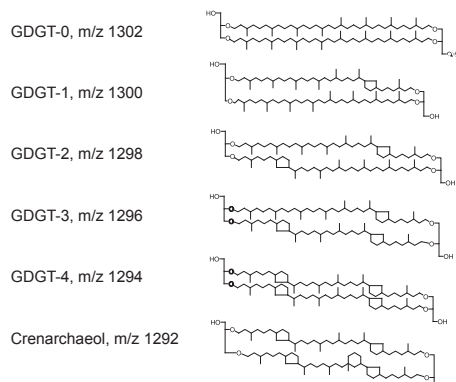
1364

1365

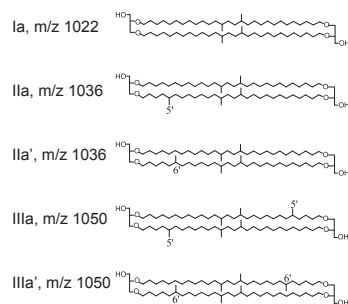


1366 **Figure 2.** Chemical structures of the relevant isoGDGTs, brGDGTs and brGMGTs and
1367 their terminology as described in this study. For the terminology of the brGMGTs, for
1368 which the exact chemical structure is still unclear, we follow Baxter et al. (2019), since
1369 we identify the same isomers (see Figure S2 for a chromatogram).
1370

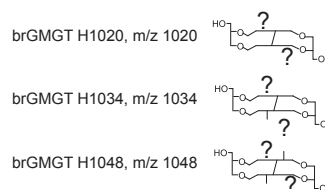
Isoprenoidal GDGTs



Branched GDGTs



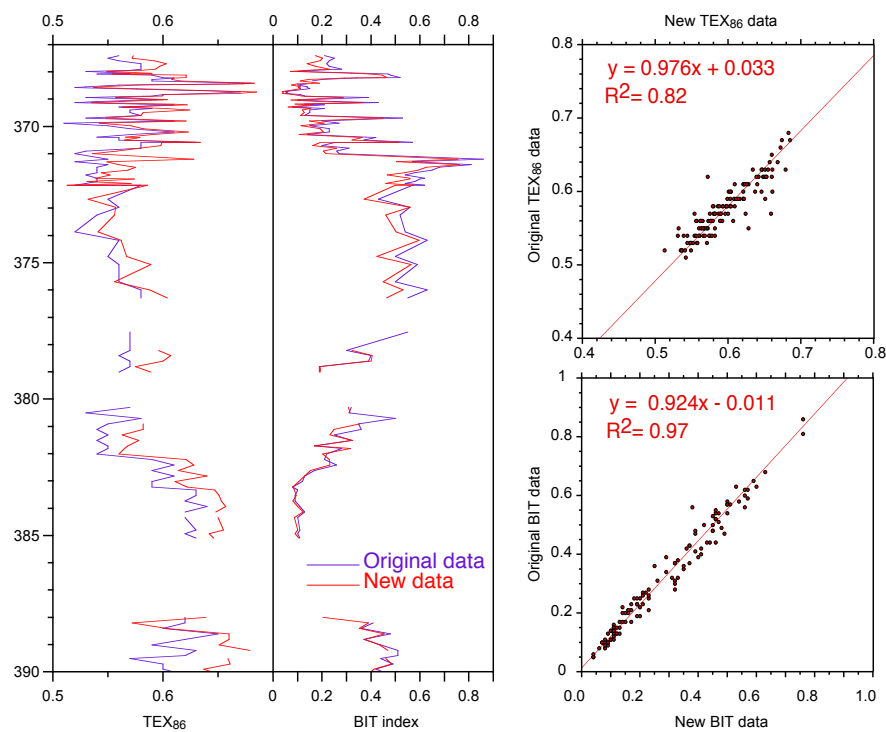
Branched GMGTs



1371

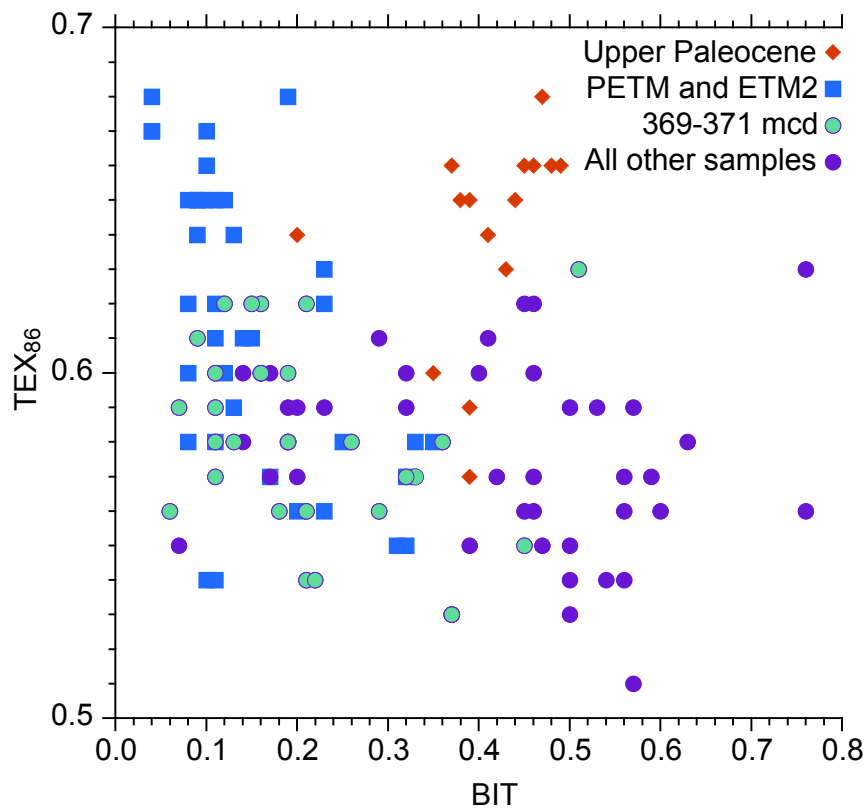


1372 **Figure 3.** Comparison of the original GDGT dataset of the upper Paleocene and lower
1373 Eocene of ACEX Hole 4A (Sluijs et al., 2006; Sluijs et al., 2009) and the new data
1374 generated according to the latest chromatography protocols.





1376 **Figure 4.** Comparison between BIT index values and TEX_{86} for various intervals
1377 spanning the upper Paleocene and lower Eocene of ACEX Hole 4A.



1378

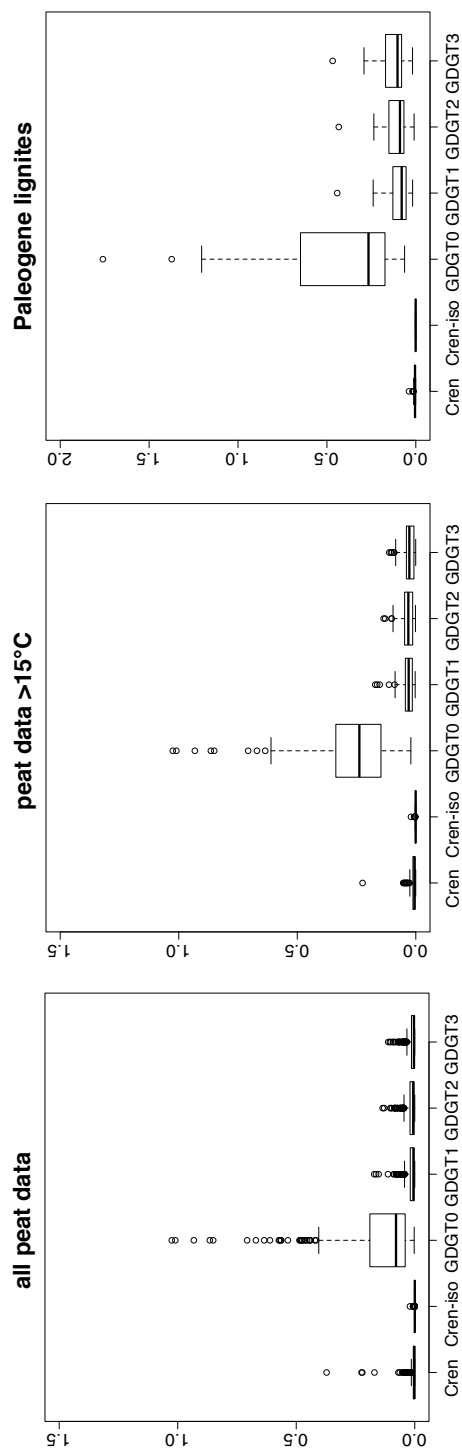


Figure 5. The distribution of various isoGDGTs relative to the total brGDGTs in modern peats and Paleogene lignites (Equation 9), used to assess potential isoGDGT contributions to the ACEX samples.

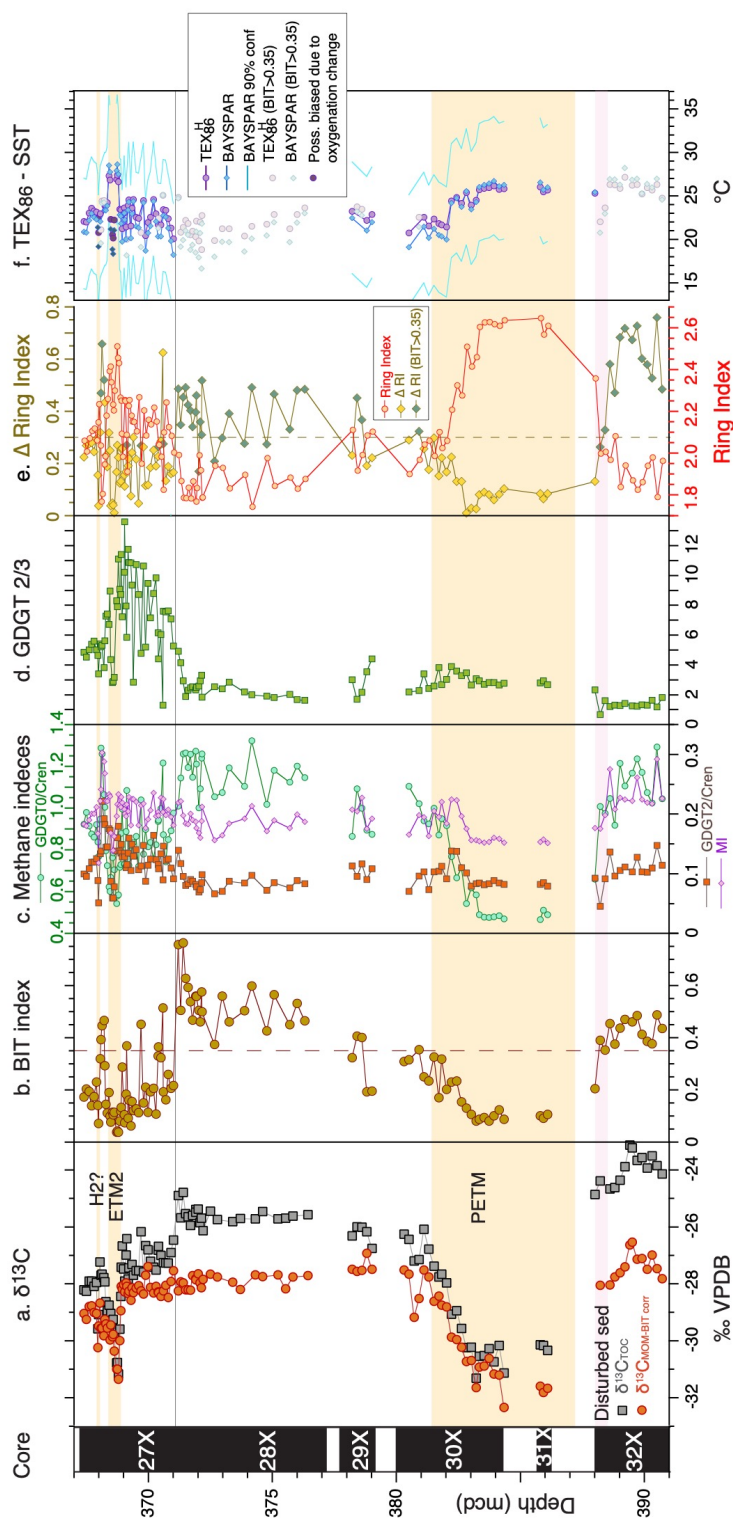


Figure 6. Branched and Isoprenoid GDGT records across the upper Paleocene and lower Eocene of ACEX Hole 4A. a. carbon isotope stratigraphy (total organic carbon record from Sluijs et al., 2006 and 2009; marine organic matter record from Sluijs and Dickens (2012)), b. BIT index (equation 2), c. indices indicative of anaerobic archaeal methanotrophy (MI index (equation 3) and GDGT-2/Crenarchaeol), and methanogenesis (GDGT-0/Crenarchaeol), d. GDGT2-GDGT3 ratio, e. Ring Index (equation 5) and Δ Ring Index, f. TEX_{86} (equation 1) calibrated to sea surface temperature using a non-linear calibration TEX_{86}^H calibration (Kim et al., 2010) and the BAYSPAR method, which is based on a linear calibration (Tierney and Tingey, 2014).



1382

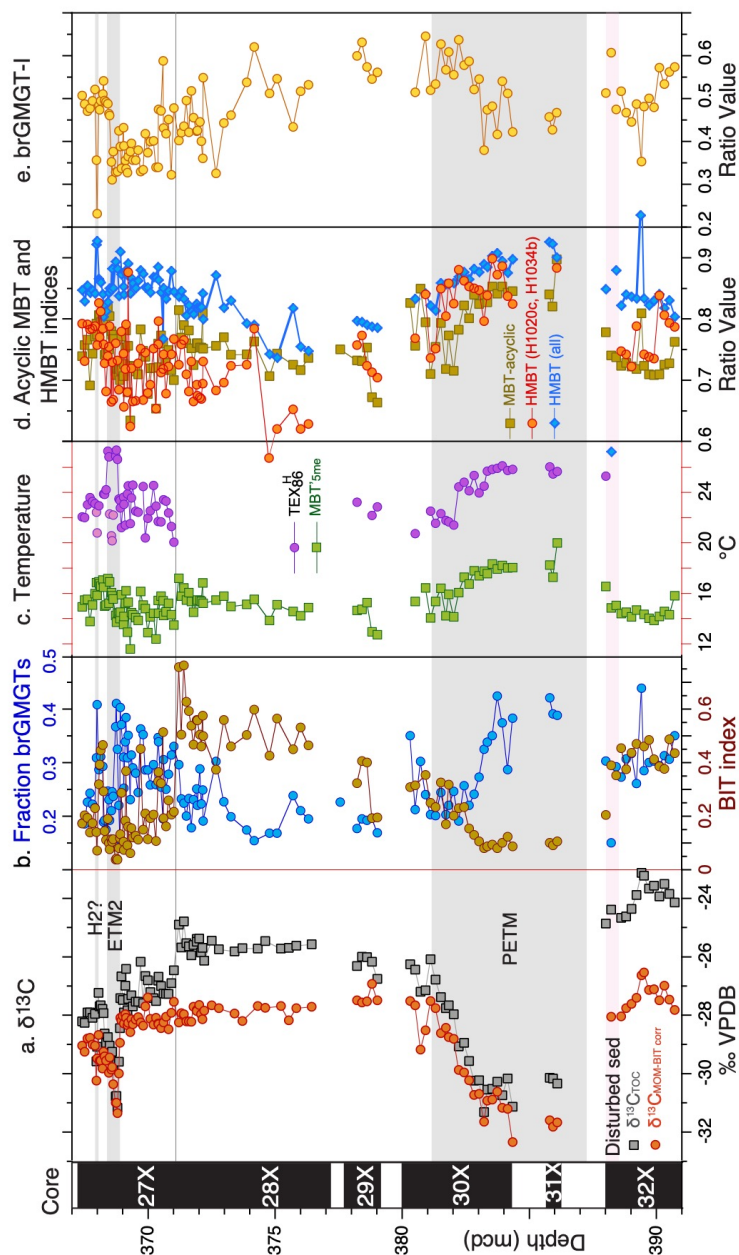


Figure 7. Branched GMT records across the upper Paleocene and lower Eocene of ACEX Hole 4A. a. carbon isotope stratigraphy (total organic carbon record from Sluijs et al., 2006 and 2009; marine organic matter record from Sluijs and Dickens (2012)), b. fraction of brGMTs of the total branched GDTs and GMTs and BIT index (equation 2), c. MBT_{5me} record (Willard et al., 2019) and TEX₈₆^H, d. MBT_{acyclic} (equation 6) and H-MBT based on all isomers detected with m/z 1020 and m/z 1034 (H-MBT all; equation 7) and based on H1020a and H1034b (H-MBT H1020a, H1034b), e. brGMT-1 record (equation 8).